AAPS PharmSciTech (2022) 23:300
https://doi.org/10.1208/s12249-022-02448-w

RESEARCH ARTICLE

Insights into the Role of Compendial/Biorelevant Media on the Supersaturation Behaviour of Drug Combination (Drug-Drug Interaction) and Precipitation Inhibition by Polymers

Prachi Joshi[1] · **Abhay T. Sangamwar**[1]

Received: 20 August 2022 / Accepted: 27 October 2022
© The Author(s), under exclusive licence to American Association of Pharmaceutical Scientists 2022

Abstract

Combination drug therapy (CDT) plays an immense role in the treatment of various diseases such as malaria, hypertension, cancer, HIV-AIDS, helminthiasis, and many more. However, *in vitro* drug-drug interaction (DDI) is not well reported for better efficacy of CDT. In DDI one drug may enhance the precipitation of other drugs thereby reducing the advantage of CDT. Herein, we report DDI in terms of *in vitro* precipitation of drugs with albendazole and mebendazole. This may be the first report to propensate the possibility of either drug precipitation in the combination. These drugs are categorized into BCS class II weak base and hence have tendency to precipitate in the gastrointestinal tract. The objective of this study is to find precipitation of drug combinations in different compendial and biorelevant media (deionized water, phosphate buffer pH 6.8, FaSSIF, and FeSSIF) and screening of the polymers for precipitation inhibition. Nine polymers were investigated at three different concentrations in terms of their drug-polymer solubility, *in vitro* precipitation behavior, induction time, SHC, and droplet size. Although, all the polymers inhibit the precipitation of drugs, the extent of precipitation inhibition for Soluplus is high. The obtained drug-polymer precipitates were filtered, dried, and analyzed for amorphous/partial amorphous form using polarised light microscopy (PLM), differential scanning calorimetry (DSC), and powder X-ray diffractometry (PXRD). The drug-polymer interaction was examined using Fourier transform infrared (FTIR) spectroscopy and nuclear magnetic resonance (NMR) revealing the effect of polymers on drug precipitation. These insights may further be used in the formulation of CDT for helminthiasis management.

Keywords drug combination · drug-drug interaction · drug-polymer · interplay · *in vitro* polymers · precipitation · supersaturation

Abbreviations

ABZ	Albendazole
MBZ	Mebendazole
WHO	World Health Organization
AMB	Albendazole-mebendazole
DW	Deionized water
PB	Phosphate buffer pH 6.8
FaSSIF	Fasted state simulated intestinal fluid
FeSSIF	Fed state simulated intestinal fluid
PVA	Polyvinyl alcohol
PVP K10	Polyvinyl pyrolidone K10
PVP K30	Polyvinyl pyrolidone K30
PVP K90	Polyvinyl pyrolidone K90
PVP VA64	Polyvinyl pyrolidone vinyl acetate
SDS	Sodium dodecyl sulfate
SOL	Soluplus
POLX	Poloxamer/Pluronics F68
KOLLI	Kolliphor/Solutol HS15
PIs	Precipitation inhibitors
STH	Soil-transmitted helminths
PLM	Polarized light microscopy
DLS	Dynamic light scattering
FTIR	Fourier transform infrared spectroscopy
NMR	Nuclear magnetic resonance

Introduction

Combination drug products have been used extensively for increasing pharmacological effects either by synergistic or additive effects of the drugs. However, the

✉ Abhay T. Sangamwar
abhays@niper.ac.in

[1] Department of Pharmaceutics, National Institute of Pharmaceutical Education and Research (NIPER), S.A.S. Nagar, Mohali, Punjab 160062, India

Published online: 15 November 2022

biopharmaceutical performance of the combination drug therapy is not well understood. Drug-drug interaction within the formulation may affect the biopharmaceutical performance of either drugs. Supersaturated drug delivery systems are largely practiced to mimic the biopharmaceutical performance of drugs *in vivo*. These systems provide an answer to tackle the issues of solubility and permeability of the drugs. However, intestinal precipitation of drugs is a major issue in the prolonged supersaturation of the drugs. The selection of suitable excipients to inhibit this precipitation is challenging. The drug-drug interaction in combination drug therapy may augment the precipitation of either drug *in vivo*. The diminutive amount of literature is available on the supersaturation behavior of drug combinations and how they affect the supersaturation and absorption behavior of each other. An understanding of *in vitro* supersaturation behavior of combination drugs may help in developing a tailor-made supersaturated drug delivery systems [1–6].

Albendazole and mebendazole are enlisted by World Health Organisation (WHO) under the essential medicine list (2021) [7] for the treatment of helminthiasis. WHO recommends preventive chemotherapy [8] to prevent the worm burden of helminthic infection with periodic use of anthelminthic medicine [9, 10]. However, limited number of drugs are available for the treatment of helminthic infection, and also some of these drugs have low efficacy against infection. There are chances of the development of resistance too. Hence, to control helminthiasis, we either need new anthelminthic molecules or combinations of existing ones. The existing scenario of the high budget requirement for new drug discovery and less than 1% of the global budget [11] is spent on helminthic research due to the neglected disease led to existing drug combinations screened against helminthiasis. The albendazole and mebendazole combination has good promiscuity. Both drugs are broad-spectrum anthelminthic, mostly used in preventive chemotherapy, and are well tolerated with less side effects. Additionally, it is common for an individual (especially children) to get infected with different helminthic infections (whipworm, hookworm, and roundworm) at a time [12]. MBZ has good efficacy against whipworm whereas ABZ is superior against hookworm. Hence, combinations of ABZ and MBZ may intensify the effect against these infections [12–15]. MBZ is therapeutically active in its native form whereas ABZ needs to get converted to its active metabolite albendazole sulfoxide (ABZSO) in the liver. This suggests that MBZ shows its anthelmintic activity followed by ABZSO [12].

The oral bioavailability of ABZ is 5% and MBZ is < 10% [16, 17] which warranted a high dose for the desired therapeutic effect, welcoming the side and toxic effects [18]. Additionally, ABZ [19] and MBZ [17] have the tendency to precipitate as they move from gastric to intestinal (site of action) pH due to their weakly basic nature. The objective of the current study is to prevent the precipitation of these drugs in the small intestine, where they are supposed to initiate antihelminthic activity. We initially find the effect of media (water, phosphate buffer pH 6.8, FaSSIF, FeSSIF (early) on the precipitation behavior of AMB (combinations of ABZ and MBZ). The precipitation studies of ABZ and MBZ were performed alone and in combination. The precipitation of both drugs was enhanced in presence of each other. Further studies were performed such as equilibrium solubility, precipitation kinetics, nucleation induction time, dynamic light scattering, and supersaturation holding capacity to the suitable precipitation inhibitor (PI) for this combination, as a single experimental study may provide false positive polymer. Based on the above results, Soluplus was an effective PI followed by PVP K90 and Kolliphor HS 15. The selected PIs were scrutinized for solid-state characterization such as thermal (DSC), crystallographic (PXRD), and microscopic (PLM) analysis to reveal the effect of polymers on solid state properties of AMB. Moreover, drug-polymer interactions were displayed using proton nuclear magnetic resonance (NMR) and fourier transform infrared (FT-IR) spectroscopy.

Material

Albendazole and mebendazole generously gifted by SU Pharma Chem Pvt. Ltd. Gujrat. Soluplus (90–140,000 g/mol), PVP K90 (900,000–1,300,000 g/mol), PVP K30 (35,000–51,000 g/mol), and Kolliphor HS15 (170,000 g/mol) were provided by BASF Mumbai. PVA (87–90% hydrolyzed) (30,000–70,000 g/mol), PVP K10 (10,000 g/mol), and Poloxamer F68 (8400 g/mol) were purchased from Sigma-Aldrich Chemical Ltd. Mumbai. PVP VA64 (45,000–70,000 g/mol) was obtained from Signet Chemical Corporation Pvt. Ltd. Mumbai. Sodium taurocholate, maleic acid, and lecithin were purchased from Himedia, Mumbai. HPLC grade methanol and ACN were purchased from Central Drug House Ltd. (CDH) in New Delhi. All chemicals used were of analytical grade. The chemical structure of drugs and polymers is provided in supplementary data Fig. S1.

Methods

Preparation of Biorelevant Media

The biorelevant media for FaSSIF and FeSSIF (early stage) was prepared as described in the literature [20]. Firstly, blank FaSSIF and FeSSIF (media without bile components) were prepared, then sodium taurocholate was added and dissolved using a magnetic stirrer (Daihan Instruments, South Korea) till no solid particle is visible, subsequently, other components (lecithin and GMO) were dissolved in DCM and added in a dropwise fashion. The solution was stirred under heating to evaporate the DCM. The solution was filtered

using cellulose filter papers (pore size 11 µm) before use. Media were stored at 4°C temperature and consumed within 2–3 days after preparation. The composition of both media is provided in supplementary data (Table S5).

Supersaturation Studies

The solvent shift method was opted for the generation of a supersaturated solution. ABZ was dissolved in glacial acetic acid: methanol (1:1) whereas MBZ was dissolved in 0.02 M acidic methanol. The microarray plate method was opted for the study. Preheated test media of 300 µL was added into the wells, to which 10 µL of AMB (1:1) solution was added. The plate was subjected to Spectramax M2^e (Molecular devices) spectrophotometer (Fig. S4) for analysis for 4 h at a reading interval of 60 s and shaking of 5 s before reading [21]. The absorbance wavelength was 310 nm for MBZ and 350 nm for ABZ. Similarly, the experiment was performed in presence of polymers and different precipitation media.

Saturation Solubility Studies

Saturation solubility studies were performed in deionized water, phosphate buffer pH 6.8, FaSSIF, and FeSSIF (early stage). Drug equilibrium solubility was performed with and without polymers. Polymers were pre-dissolved in the test media at 3 different concentrations (0.05, 0.2, and 1.0% w/v, respectively). Excess of AMB was added into the glass vials possessing pre-dissolved polymeric solution, the samples were vortexed for proper mixing of drug into the solution. Samples were equilibrated at 37 ± 0.2°C and 100 rpm in a water shaker bath for 24 h. A sample of 1 mL was withdrawn, centrifuged (SPINWIN™, Microcentrifuge) at 10,000 rpm for 10 min), filtered (0.2 microns), and suitably diluted for HPLC analysis. The HPLC data is represented in the supplementary information (Table S1-S4 and Fig. S2-S3).

Nucleation Induction Time and Supersaturation Holding Capacity (SHC)

Experimentally, it is difficult to detect the time at which nucleation occurs in the precipitation media as it differs from the method of detection. Nuclei should grow to a detectable range above critical nuclei for identification. As the nucleation occurs and matures up to a measurable range, a drop in absorbance will occur which is considered as the onset of crystallization. In this study, the nucleation induction time was calculated using the regression line method. Regression lines were drawn to the two distinct linear regions of the precipitation curve, and their point of intersection was considered as induction time [22].

SHC [22, 23] was calculated as the ratio of area under curve (AUC) difference between 10 and 50 min in the presence and absence of polymers. It is the crucial time interval for the occurrence of nucleation induction. The AUC was calculated using OriginPro 9.1 software. The SHC was calculated using Eq. 1.

$$\mathrm{SHC} = \frac{\mathrm{AUC}\,(50-10)\text{presence of polymer}}{\mathrm{AUC}\,(50-10)\text{absence of polymer}} \quad (1)$$

Particle Size and Zeta Potential Analysis

To the 10 mL of preheated test media (with and without polymers) placed in a water shaker bath (Daihan Instruments, South Korea) operating at 37 ± 0.2°C at 100 rpm, drug solution was added in a dropwise fashion. The sample was withdrawn after 5 min, suitably diluted, and the droplet size and zeta potential were analyzed using Zetasizer Nano ZS (Malvern instruments) [24]. The measurements were taken in a disposable cuvette at the backscatter angle of 173°.

Solid State Characterization

The obtained precipitates from each media were filtered using Whatman™ filter paper (11 microns) which were further dried in the oven at 40°C and then stored in desiccators until further analysis.

Polarised Light Microscopy (PLM)

PLM is the primary step toward solid-state characterization. It is the simplest and reliable approach to understand the particle morphology. The sample was placed on the clean glass slide, and a drop of silicone oil was added and dispersed on the slide with the help of a coverslip for the proper spreading of the sample. Lecia DMLP polarized microscope (Lecia Microsystem Wetzlar GmbH, Germany) was used for the experiments. The images were observed under 20 × magnification and captured using Lecia DC 300 camera operating with Lecia IM50 image manager software.

Differential Scanning Calorimetry (DSC)

DSC analysis was performed to understand the thermal behavior of AMB precipitates in the presence and absence of polymers. The instrument used for analysis was Linseis Chip DSC 10 equipped with Linseis TA (thermal analysis) evaluation software. The system was calibrated with indium and tin. About 3–4 mg of the sample was weighed on the aluminum crucible and placed on the sample cell purged with nitrogen with the flow rate of 200–250 mL/min. The samples were analyzed with a heating rate of 10°C/min up to 260°C.

Powder X-ray Diffraction (PXRD)

Powder X-ray diffraction is used to analyze the solid-state nature of the drug and drug-polymer precipitates. The instrument used for analysis is Rigaku SmartLab, Japan. The instrument radiation source was Cu Kα ($\lambda = 1.54$) operated at 40 kV/50 mA with a scan speed of 10°/min and step width of 0.02° in the range of 3–40 θ.

Fourier Transform Infrared Spectroscopy (FTIR)

FTIR is the characterization tool to understand the drug-polymer interaction which is represented in terms of change in functional group wavenumber. The samples were analyzed using FTIR (Perkin Elmer, Buckinghamshire, UK) coupled with spectrum v3.02 software. The disk was prepared by mixing KBr and drug-polymer precipitates using a hydraulic press. The samples were scanned within the range of 4000 to 700 cm^{-1}.

Nuclear Magnetic Resonance (NMR)

Around 5–6 mg of sample (drug, polymer, and drug-polymer precipitates) was dissolved in deuterated DMSO, transferred into an NMR sample tube and subjected for analysis. Sample analysis was performed using Bruker 500 (UltraShieldTM, Germany) operating at 500 MHz at room temperature. Spectra were recorded over a spectral range of 15 ppm. Data was analyzed using Mestronova spectrum software.

Results and Discussion

Saturation Solubility Studies

As shown in Fig. 1, solubility was lowest in phosphate buffer pH 6.8 (MBZ 1.04 µg/mL and for ABZ 1.71 µg/mL, respectively), followed by deionized water (MBZ 2.471 µg/mL and for ABZ 1.754 µg/mL, respectively). The drug solubility increases in biorelevant media because of the presence of bile salts and lipid components. In FaSSIF, there was a slight increment in drug solubility; however, the difference is not significant the MBZ and ABZ solubility was 3.17 and 4.37 µg/mL, respectively. Moreover, in FeSSIF, a significant leap in saturation solubility was presented, the solubility of MBZ and ABZ was 17.51 and 25.96 µg/mL, respectively. The solubility results are in correlation with the literature, wherein it is reported that MBZ and ABZ absorption increases in the presence of fat. Most of the polymers have shown the positive effect on the drug solubility. The degree of enhancement in solubility was dependent on the polymer properties and concentration.

Polyvinyl alcohol works like both anionic (solubilizer) and non-ionic (less variability) polymers because of its tunable density between hydrogen bond donors and acceptors with polyvinyl backbone [25]. However, the effect of PVA on the solubilization of ABZ and MBZ was not significant. The possible reason for such behavior is because of the higher degree of hydrolysis makes the nature of PVA more crystalline which makes its solubilization slow in the media. PVP (K10, K30, K90, and VA64) polymers have hardly increased the drug solubility in water; however, PVP K30 and PVP VA64 slightly increased the solubilization of ABZ and MBZ in phosphate buffer pH 6.8 and FaSSIF at a concentration of 0.05% w/v. Soluplus is a polyvinyl caprolactam–polyvinyl acetate–polyethylene glycol graft copolymer with amphiphilic nature, its bifunctional properties make it an excellent candidate for enhancing solubilization of poorly soluble drugs. In water, Soluplus enhanced the solubilization of ABZ and MBZ at higher concentrations (1% w/v), whereas at lower concentrations (0.05 and 0.2% w/v) the enhancement was not significant. SDS is an anionic surfactant which significantly enhanced the solubility of ABZ and MBZ at 1.0% w/v concentration in water and FaSSIF.

Polymers such as Soluplus, SDS, Kolliphor, and poloxamer are more effective because they belong to the surfactant category. Both ABZ and MBZ have poor wettability and the principle mechanism through which surfactants act is either by micelle formation or by increasing the drug wetting property. Further, the polymer chain alignment may differ depending on the type of solvent and its pH [26], which also alters the solubilization efficacy of the polymers. The solubility enhancement was proportional to the polymer molecular weight.

The possible reason for the decrease in drug solubility with the increase in polymer concentration can be because the long chain polymers entangle with each other because of which it becomes difficult for the solvent to penetrate which makes them to dissolve slowly. Polymer solubility can be affected with its molecular weight, the pH of the solution [26], and the presence of salts [26, 27].

In Vitro Precipitation Studies

Due to the weakly basic nature of AMB, they have a propensity to precipitate at alkaline pH. However, in biorelevant condition, the precipitation was limited due to the presence of bile and lipid components. As presented in Fig. 2, both the drugs exhibited rapid precipitation, which may be the probable reason of less absorption and low intraluminal concentration to permeate the gastromucosal layer for therapeutic effect. However, the drug precipitation was much more rapid in presence of each other as compared to alone. The concentration *vs* time profile of drug and polymers was shown in Fig. 3. The precipitation

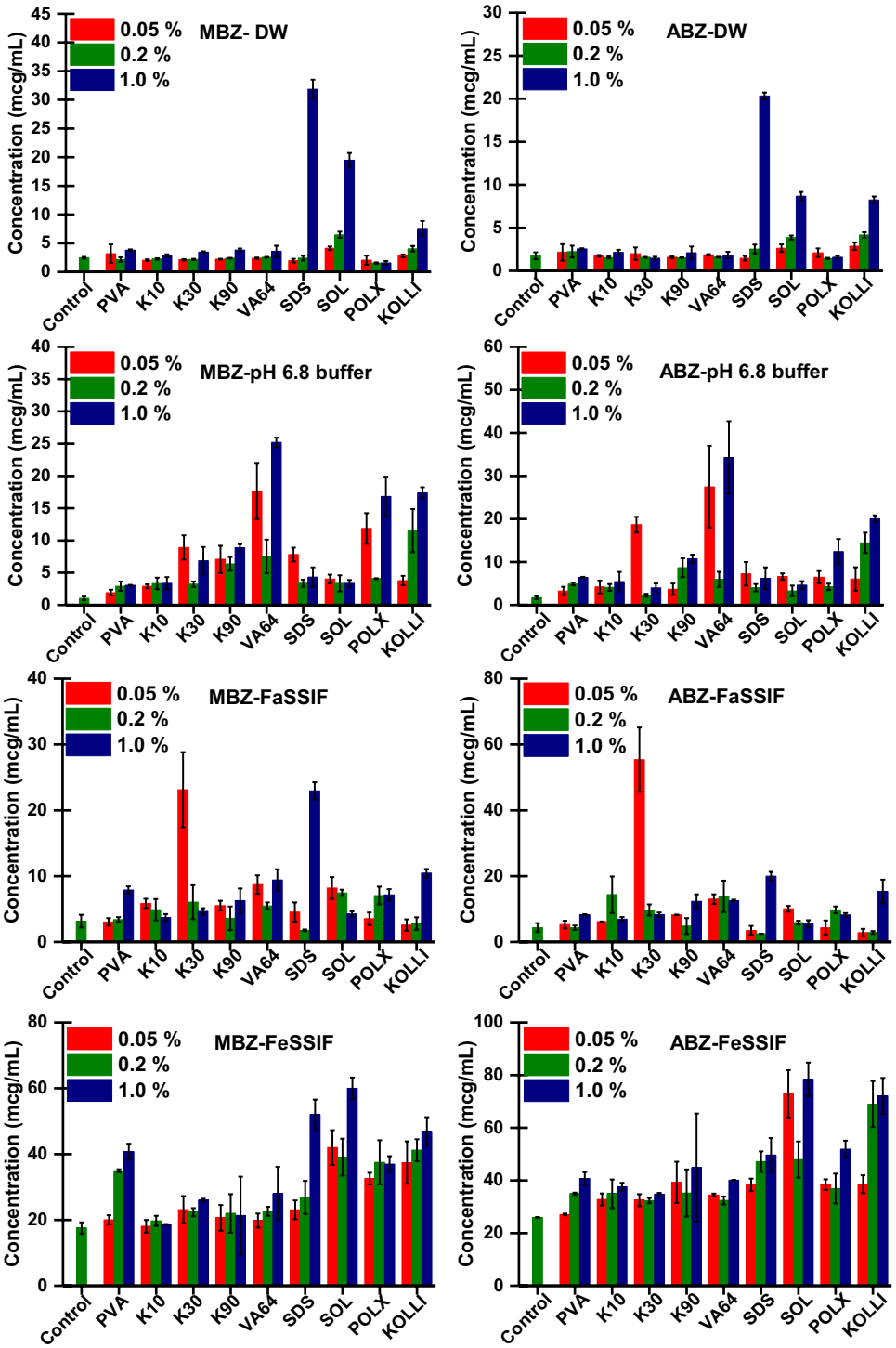

Fig. 1 Graphical representation of saturation solubility of albendazole (ABZ) and mebendazole (MBZ) in the absence and presence of polymers at different concentrations (0.05, 0.2, and 1.0% w/v) using water, phosphate buffer pH 6.8, fasted state simulated intestinal fluid (FaSSIF) and fed state simulated intestinal fluid (FeSSIF)

tendency of drugs was higher in water and phosphate buffer pH 6.8, but as it move towards biorelevant media, the precipitation tendency was slightly less. All the polymers inhibited drug precipitation but the degree of supersaturation maintenance differs with polymer type and its concentration [28, 29]. The polymer molecules get associated with the drug molecules, they get adsorb on the drug surface [30] and prevent the access of drug molecules on the surface thereby performing as crystal growth inhibitors. Surfactants such as Soluplus, SDS, and poloxamer prevented drug precipitation either by forming micelles or increasing the drug-wetting property. In case of poloxamer, hydrophobic interactions can also lead towards the prevention of drug precipitation [31].

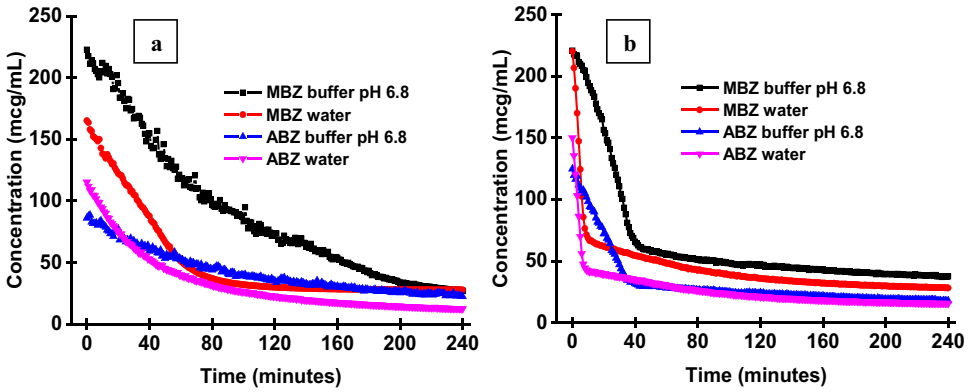

Fig. 2 In vitro precipitation profile of albendazole and mebendazole expressed as concentration *vs* time profile (**a**) alone and (**b**) in combination in compendial media

Induction Time and Supersaturation Holding Capacity (SHC)

The results for nucleation induction time are summarized in Fig. 4. ABZ and MBZ precipitate rapidly in water and phosphate buffer pH 6.8 with induction times of 12 and 13 min for the former media and 9 and 8 min for the latter media. In FaSSIF, the induction time was 6 and 9 min, and in FeSSIF, 15 and 16 min respectively. Induction time was significantly increased (> 240 min) in the presence of Soluplus and poloxamer. Additionally, precipitation media too have an effect on the induction time. In FeSSIF, the induction time was ranging from 60 to 100 min for all the polymers followed by water in which ranges from ranging from 30 to 70 min. However, in phosphate buffer, pH 6.8 induction time ranges from 15 to 50 min, and for FaSSIF it was 15–40 min. Polymer concentration also affected the induction time. In most of the conditions, induction time was augmented with increasing polymer concentration; however, with some polymers such as PVP VA64, SDS, and Kolli reverse effect was observed on induction time with increasing polymer concentration. Higher polymer concentration causes entanglement of the polymer chain making it difficult for the solvent to penetrate.

SHC is a hypothetical value which is used as a quantitative parameter to analyze the precipitation inhibition efficiency of polymers. The nuclei formation and precipitation inhibition take place in the initial phase of the supersaturation curve rather than the terminal phase. Therefore, AUC up to 50 min was taken into consideration to calculate the SHC value of PIs. Soluplus has presented the maximum SHC for AMB in all the four precipitation media. Other than Soluplus, PVP K90, poloxamer, and Kolliphor HS15 have shown good SHC. The data is provided in the supplementary information (Fig. S5).

Particle Size and Zeta Potential Analysis

The effect of PIs on the drug droplet size (represented as Z-average) using dynamic light scattering is presented in Fig. 5. When a supersaturated solution enters into an aqueous solvent system, different colloidal species are formed. The size of these species varies, such as micellar system ranges from 2 to 20 nm, nanoaggregates from 70 to 300 nm, drug-polymer nanostructures from 20 to 100 nm, and drug precipitates are > 500 nm in size. On the basis of such information, we can predict the type of colloidal species forming in the supersaturated solution. The particle size was lowest with Soluplus and SDS because of the micelle formation followed by vinyl polymers. Because of the formation of a colloidal phase droplet, size was altered with polymer type, its concentration and precipitation media. Soluplus have the lowest particle size in DW (results supported by *in vitro* precipitation studies) followed by SDS, but in phosphate buffer pH 6.8, FaSSIF, and FeSSIF results were inverse. The droplet size increases with higher polymer concentration. The particle size is dependent on the orientation of the polymer chain in the media and its concentration. However, with PVP K10, and K30, the mean particle size was higher with DW, but with phosphate buffer pH 6.8, FaSSIF, and FeSSIF the particle size reduced. For PVPVA 64, particle size was higher at all the concentrations and in each media ranging from 1000–3000 nm.

Zeta potential is the surface characteristic of the particles. It is the charge opted onto the particles surface, the charge value varies with the particle and media components. The data is presented in the supplementary information (Fig. S6), zeta potential of AMB droplets in DW is -3.2 ± 2.5 mV, in phosphate buffer (pH 6.8) -8.9 ± 0.8 mV, in FaSSIF -18.6 ± 0.7 mV and in FeSSIF -32.3 ± 1.2 mV. The media components attribute

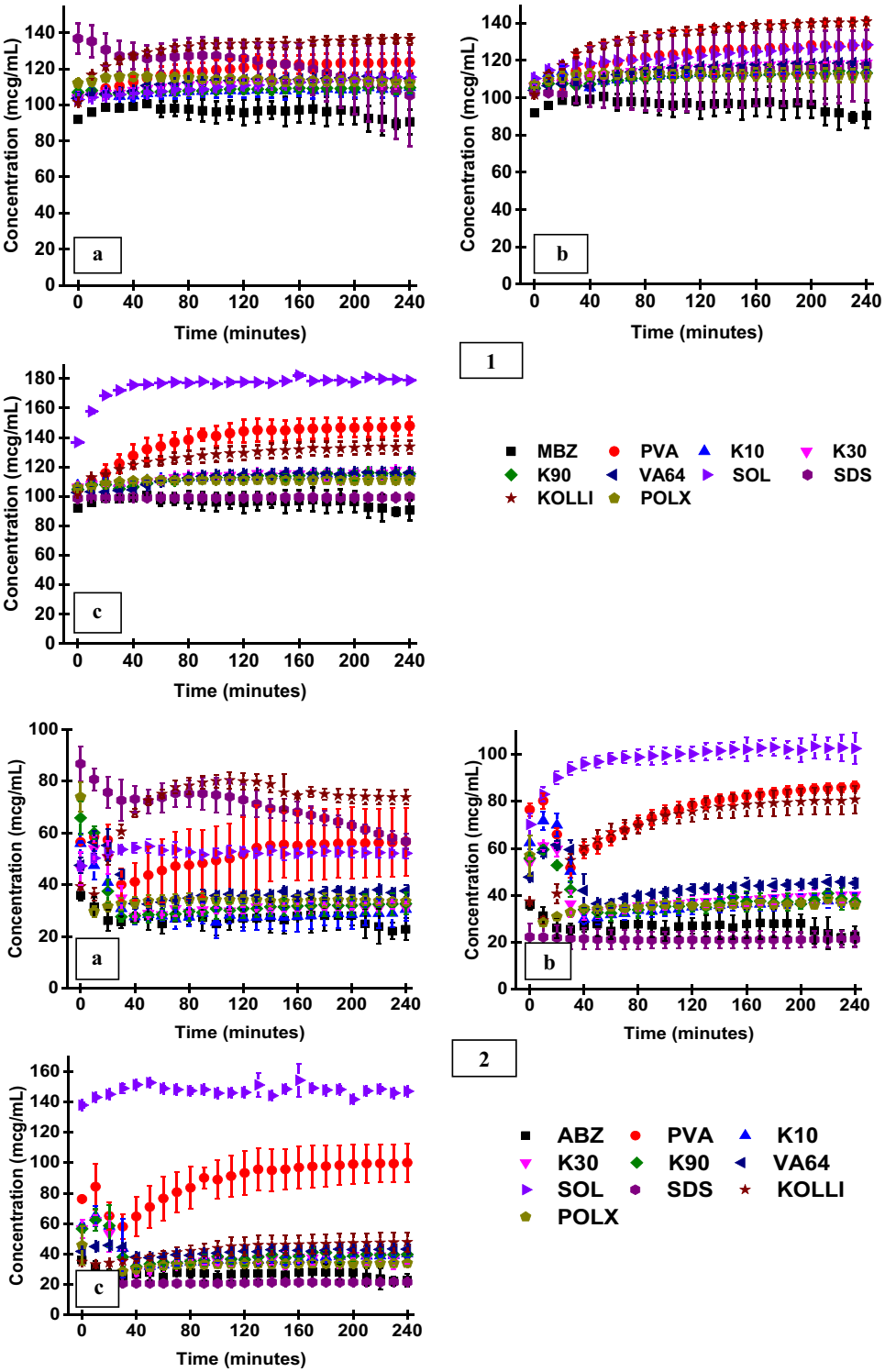

Fig. 3 Illustrating supersaturation profile of mebendazole (MBZ) and albendazole (ABZ) in terms of concentration *vs* time profile at the different polymeric concentrations in (1) MBZ-water, (2) ABZ- water, (3) MBZ-buffer pH 6.8, (4) ABZ-buffer pH 6.8, (5) MBZ-FaSSIF, (6) ABZ-FaSSIF, (7) MBZ-FeSSIF and (8) ABZ-FeSSIF. **a** represents 0.05%, **b** represents 0.2% and **c** represents 1.0% w/v of polymeric concentration

toward the change in potential by adding charge onto the droplet surface. Higher zeta potential values (±20 mV) cause repulsion between the particles (same charge) which prevents them from aggregation [32]. Although in this cause, the zeta potential value in water and buffer was very low except for SDS. The potential value was increased in FeSSIF and slightly increased with FaSSIF. The polymers SDS and polyvinyl are negatively charged and hence add a negative charge on the particle surface, while Soluplus, poloxamer, and Kolliphor are amphiphilic in nature thereby will reduce the negative charge on the AMB droplet.

Fig. 3 (continued)

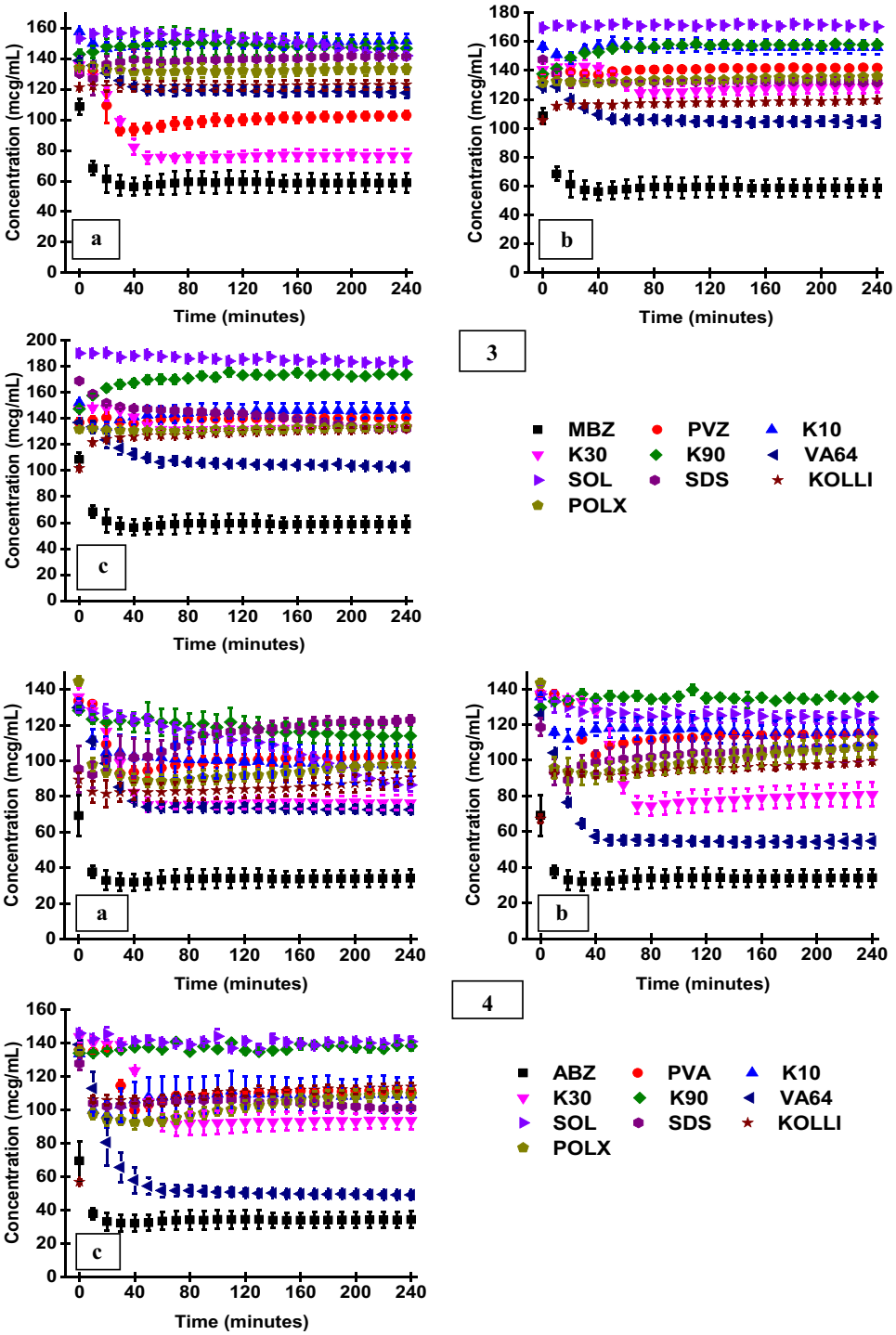

Solid-State Characterization

The solid-state characterization was carried out with Soluplus. The polymers were scrutinized on their ability to inhibit AMB precipitation, enhanced saturation solubility, nucleation induction time, droplet size, and SHC. Solid state characterization such as DSC, PXRD, and FTIR was performed with precipitates which were powder in nature.

Polarised Light Microscopy (PLM)

PLM not only reveals particle morphology but also shows the state (crystalline or amorphous) of the obtained drug-polymer precipitates. It helps to understand how polymers affect the drug crystal habit. In Fig. 6, number 1 represents non-birefringence, whereas 2 represents birefringence mode. The precipitates obtained from all the 4 media

Fig. 3 (continued)

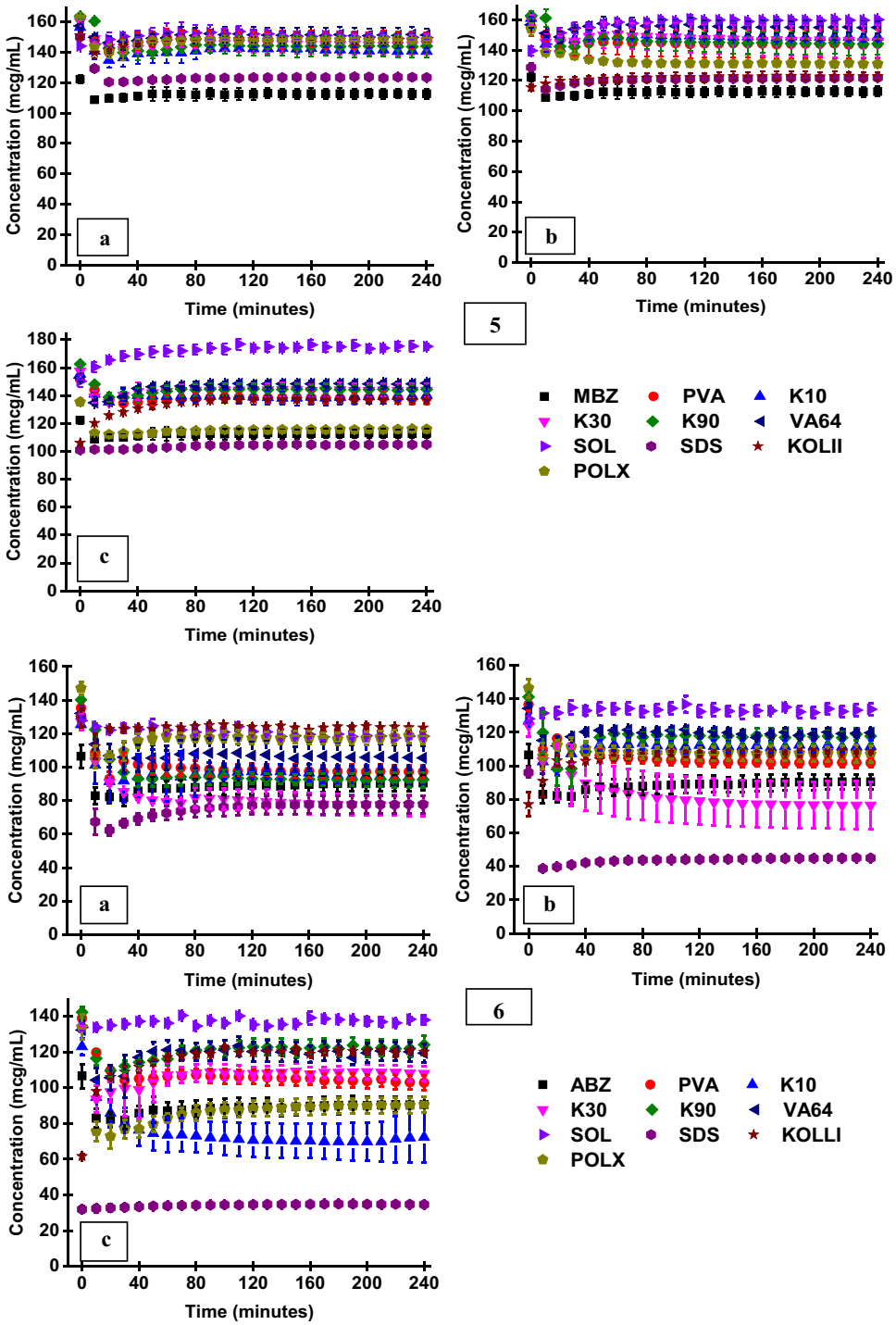

were subjected for microscopic evaluation. The microscopic images naming A, B, C, and D represent AMB-Soluplus precipitates, in four media, i.e., DW, phosphate buffer pH 6.8, FaSSIF, and FeSSIF. The acquired particles were partially crystalline to amorphous except in FeSSIF in which they were completely crystalline. The particles were irregular in shape and formed aggregates.

Differential Scanning Calorimetry (DSC)

The DSC thermogram of drug and drug-polymer precipitates is summed up in Fig. 7. ABZ showed melting at 206.1°C [33], whereas MBZ presented two melting peaks first at 216.7°C and second at 242.6°C [32] confirming their crystalline nature. The precipitates obtained from water showed

Fig. 3 (continued)

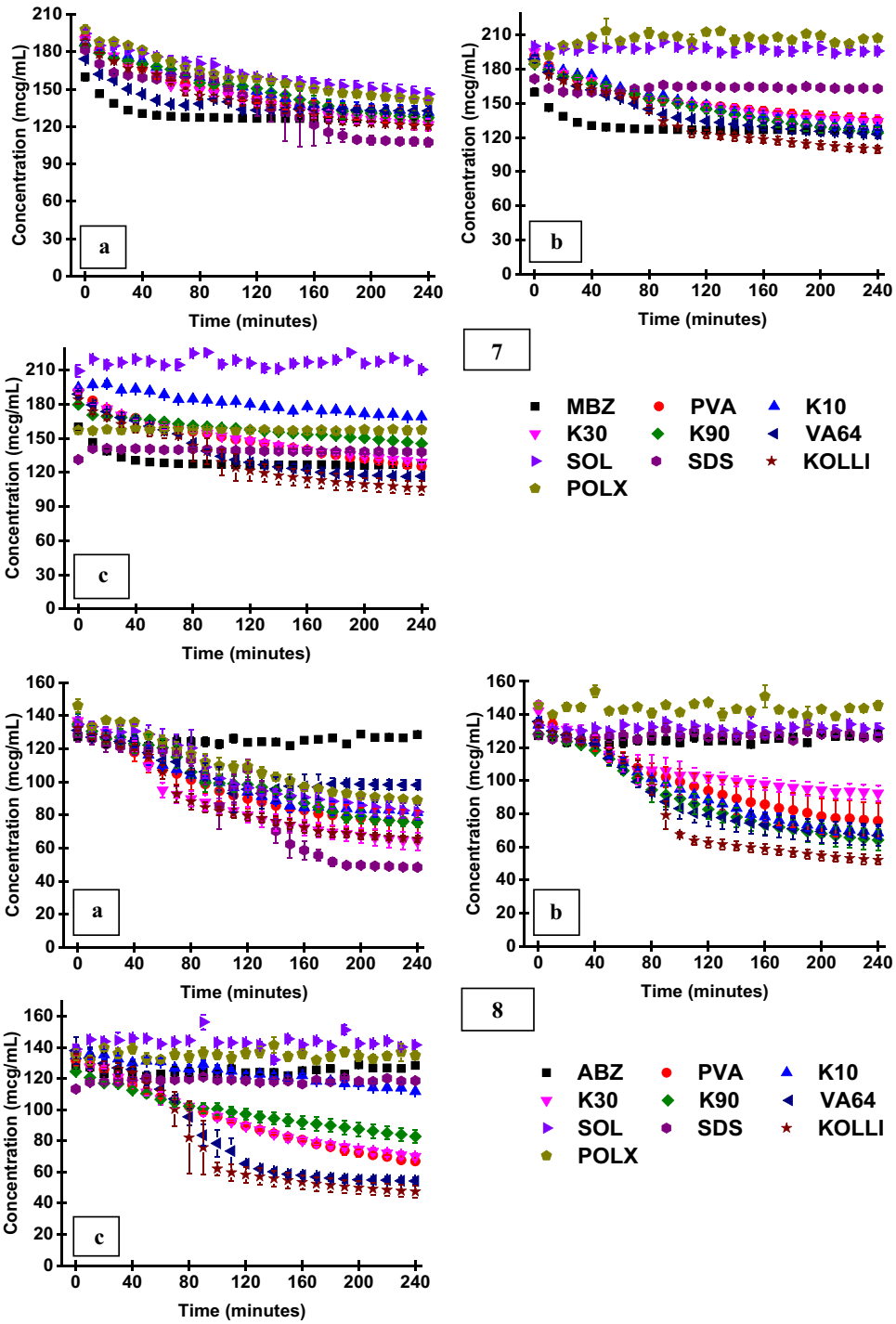

two small and broad endothermic melting peaks suggesting the presence of drug in crystalline form. In DSC thermograms of precipitates obtained from buffer, two endotherms were observed initially at 35–40°C, and a small peak was observed (present because of buffer components) followed by the second endotherm at 90–100°C that can be because of the small amount of residual solvent/moisture presents in precipitates. At 0.05% concentration, the single melting peak was observed at 195.4°C indicating drug in crystalline form. However, at polymer concentrations of 0.2% and 1.0% w/v, Tg was observed at 135.42°C and 114.7°C followed by a broad melting. This indicated the presence of drug in partial amorphous form. The precipitates procured from FaSSIF and FeSSIF displayed small and broad melting peak. The shift in melting peak also represents interaction between AMB and soluplus. The depression or shift in the melting

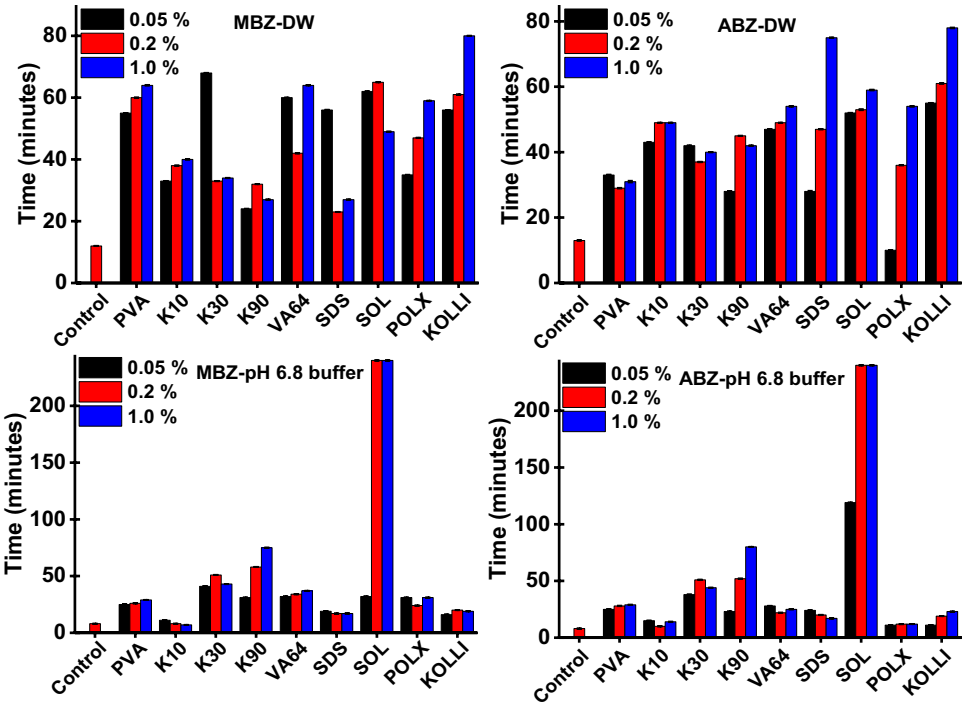

Fig. 4 Nucleation induction time of ABZ and MBZ in water, phosphate buffer pH 6.8, FaSSIF, and FeSSIF at varying polymer concentrations (0.05, 0.2, and 1.0% w/v)

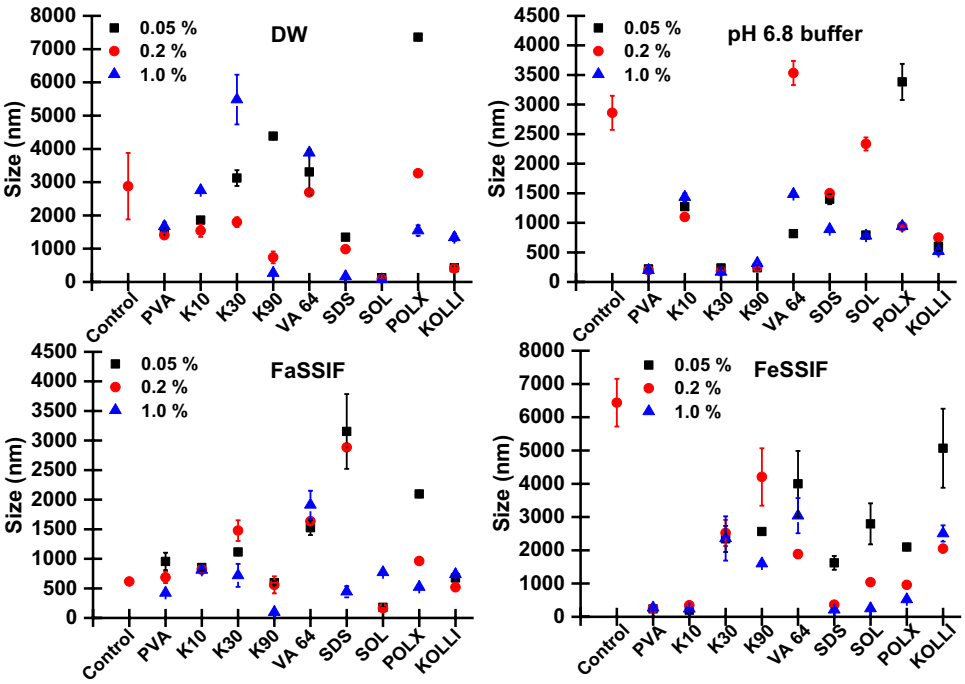

Fig. 5 Mean particle size of the AMB at different polymeric concentrations and precipitation media

peak is also a representative of drug-polymer miscibility. In phosphate buffer pH 6.8, the shift and depression in melting peak was observed with increasing polymer concentration. Similar effects were observed in biorelevant media. The results indicate the positive effect of Soluplus on the precipitation behavior of drugs by transforming them into a partial amorphous form.

Powder X-ray Diffraction (PXRD)

PXRD results are summarized in Fig. 8, representing the crystalline nature of drug with its characteristic peaks [32] and the amorphous nature of polymers. The precipitates obtained from water showed a halo pattern in PXRD indicating the conversion of drug into crystalline form. However,

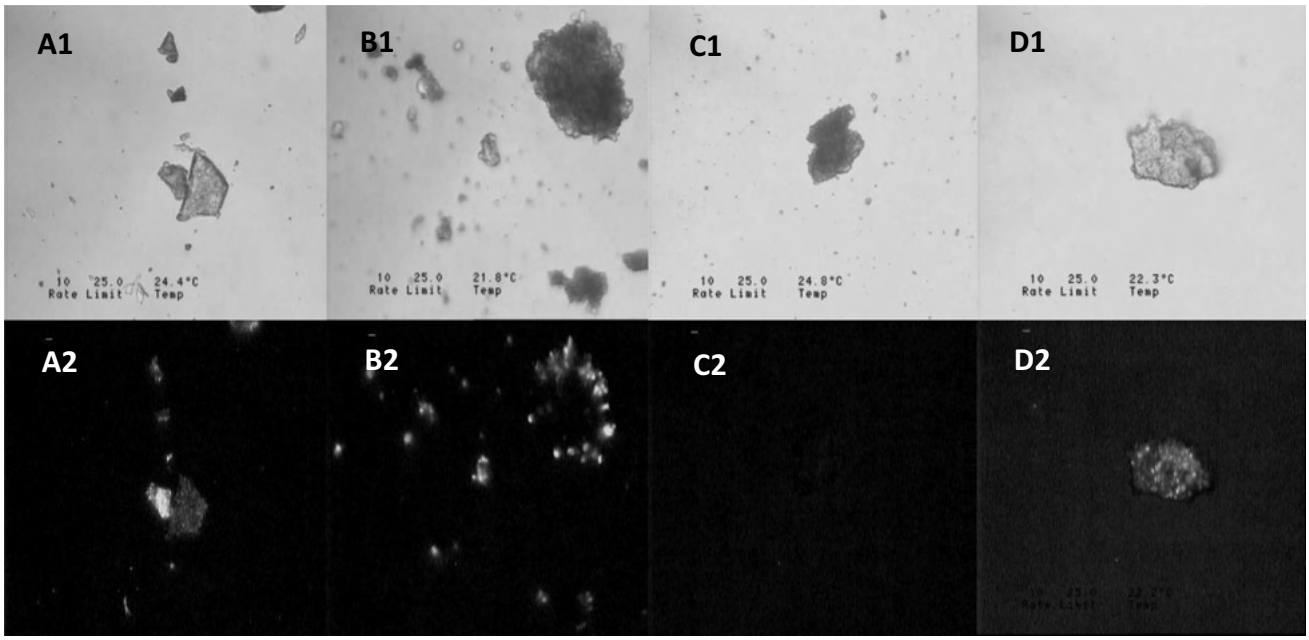

Fig. 6 Representing microscopic images of AMB-SOL precipitates. 1 represents non-birefringence mode and 2 represents birefringence mode. A represents deionized water, B represents phosphate buffer pH 6.8, C represents FaSSIF and D represents FeSSIF

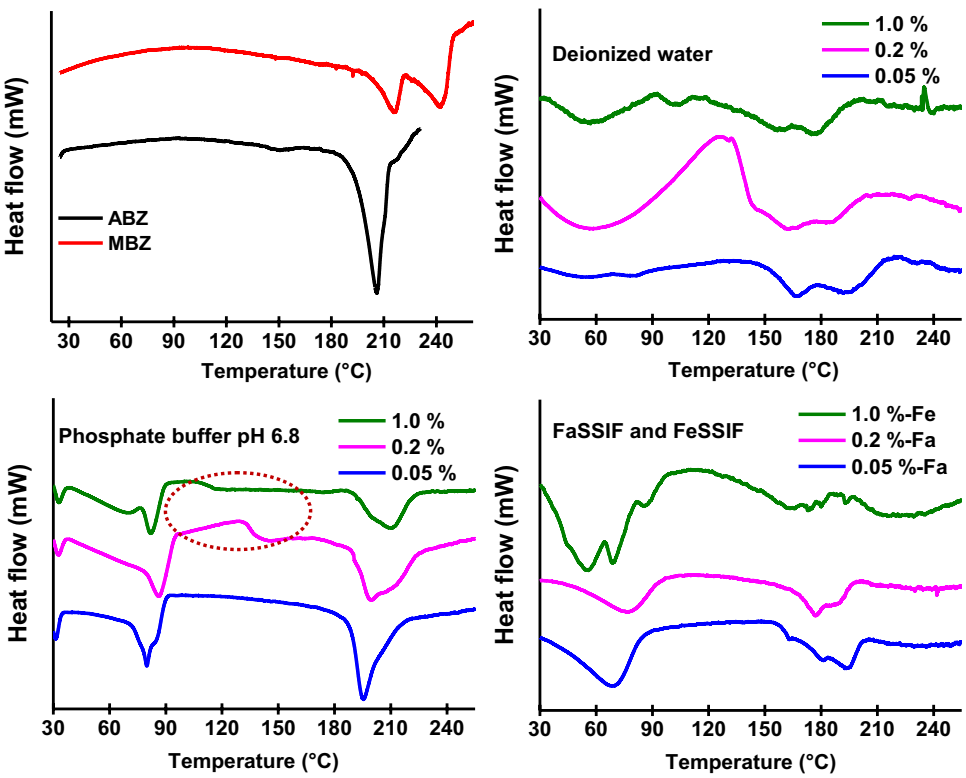

Fig. 7 DSC thermogram of drug and their precipitates in different media and polymer concentrations. The dotted circle represents the appearance of glass transition temperature in the thermogram

the results were not supported by DSC data where the small and broad melting peaks of drugs were revealed. On the other hand, the precipitates procured from the buffer displayed high-intensity peaks of buffer components, whereas peaks with low intensity are of drugs. This represents suppression of drug crystallinity with Soluplus. Moreover, in case of fasted and fed state, new peaks were observed which can be possibly due to the presence of media components

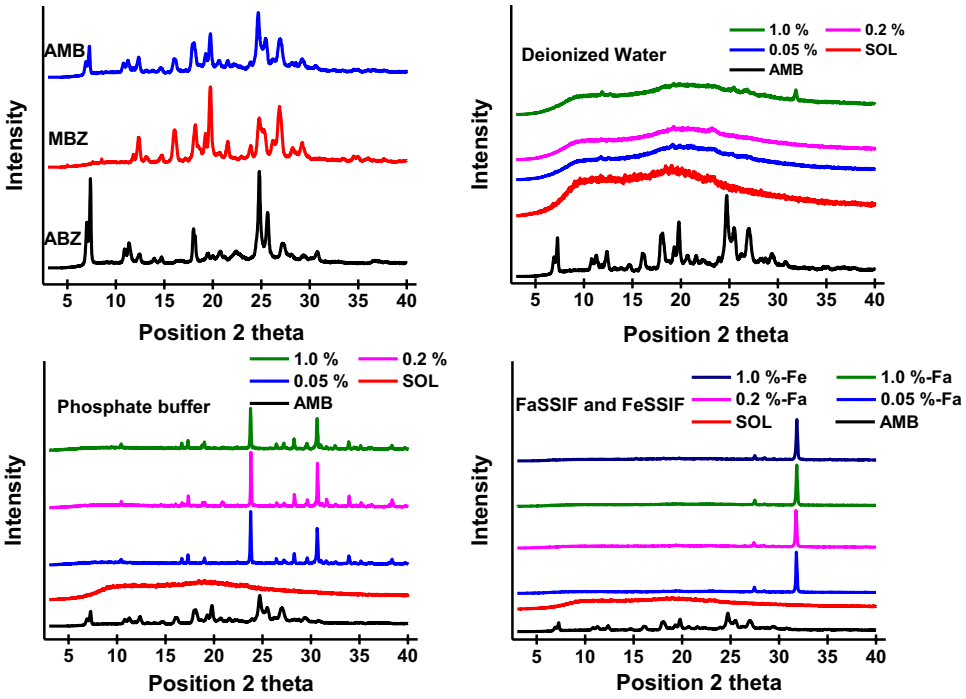

Fig. 8 PXRD diffractogram of drug and their precipitates in different media and polymer concentration

as they were not toning with the diffractrogram of drugs. Further, the PXRD results were not entirely correlating with DSC. It is difficult to detect the small amount of crystallinity using PXRD.

Fourier Transform Infrared Spectroscopy (FTIR)

FTIR reveals drug-polymer interplay in the solid state, it represents more actual picture of intermolecular interaction between drug and polymer. It provides information regarding each functional group which is involved in interaction by presenting shift or appearance/disappearance of peak/wavenumber. Here, the functional groups which are interesting are –NH and carbonyl groups; the alteration in there wavenumber represents drug and polymer interaction. The ABZ and MBZ revealed their characteristic peak at 3315.43 and 3402.44 cm^{-1} for –NH stretching and at 1711.5 and 1716.72 cm^{-1} for carbonyl stretching, respectively [34, 35]. The peak at wavenumber 1620.83 cm^{-1} represents C = C stretching (Fig. 9).

Hydrogen bonding is one of the common mechanism through which stabilization occurs; however, based on functional groups and physicochemical properties interactions can differ. In water, the peak of the –NH group was broadened and shifted towards a higher wavenumber showing their involvement in hydrogen bond formation. The C = O peak was shifted towards the lower wavenumber indicating the involvement of the carbonyl group in bonding with Soluplus. With the buffer, no significant shift in the wavenumber of the –NH peak was displayed representing the absence of hydrogen bond formation. The precipitates obtained from FaSSIF and FeSSIF exhibited a broadening and a slight shift in the –NH peak. The MBZ peak was shifted towards a higher wavenumber, whereas with ABZ the peak was shifted towards the lower wavenumber, and the carbonyl peak was broadened and slightly moved towards a higher wavenumber.

The above results indicate the interaction between drug and polymers, the shift, broadening, and disappearance of –NH, and carbonyl peaks indicate hydrogen bond formation between drug and polymer. However, in some cases where hydrogen bonding was absent, hydrophobic interactions can be the possible mechanism to maintain drug supersaturation.

Proton-Nuclear Magnetic Resonance (NMR)

Proton-NMR reveals a change in the proton environment of the groups involved in the interaction, which is represented by an alteration in the chemical shift. The NMR spectra of ABZ, MBZ, and AMB are summarized in the supplementary data (Fig. S5). The –NH group and aromatic protons were involved in the interaction. The –NH peak was shifted/disappeared with all the polymers and at each concentration showing hydrogen bond formation between AMB and polymers. For aromatic protons, change in chemical shift was observed because of the effect of the adjacent atom.

As shown in Fig. 10, shift in aromatic proton and –NH peaks was observed. Because of the presence of –NH and

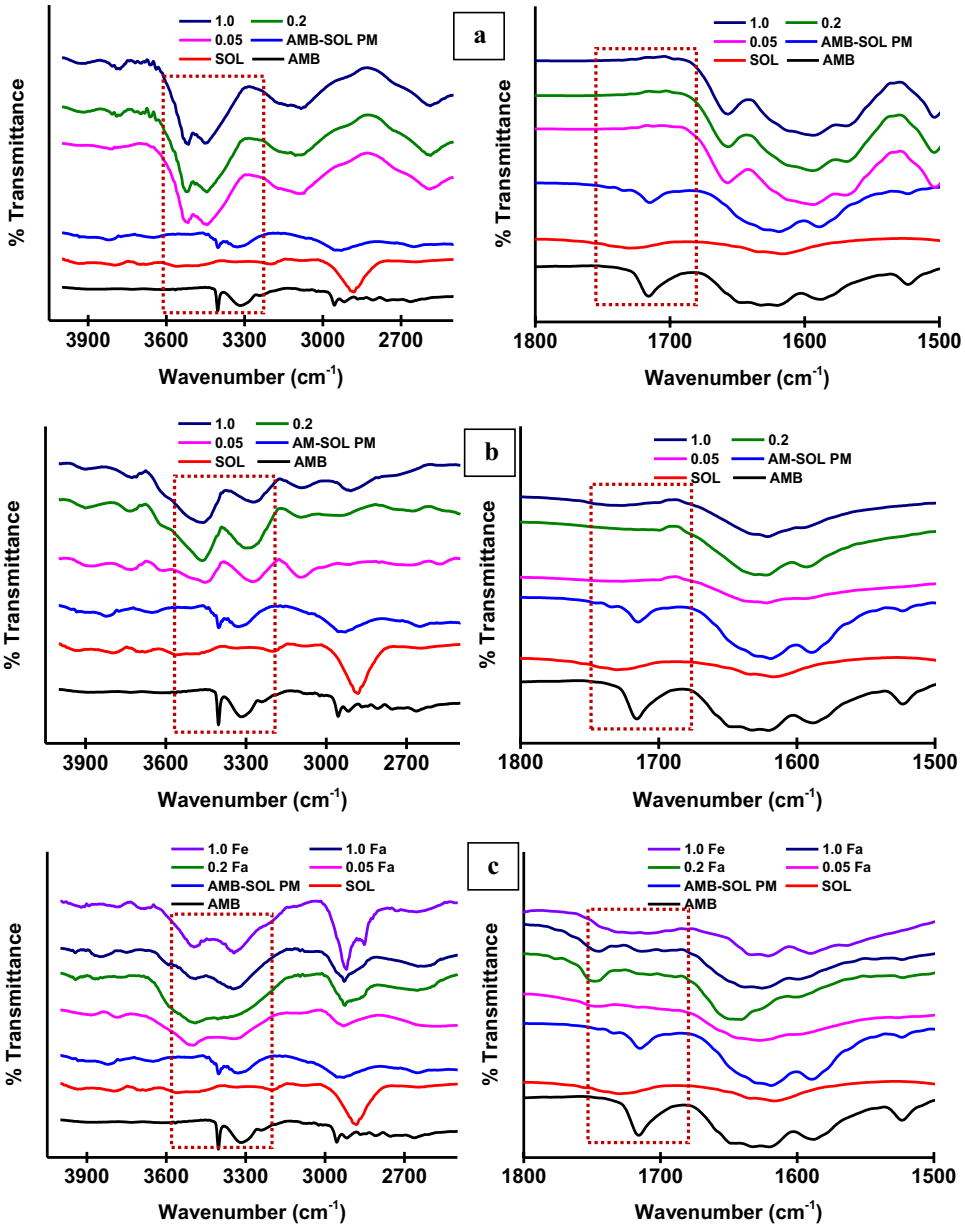

Fig. 9 FTIR overlay of drug-polymer precipitates in different media and at different concentrations. **a** represents deionized water, **b** represents phosphate buffer pH 6.8 and **c** represents FaSSIF and FeSSIF. 0.05%, 0.2% and 1.0% w/v are the polymer concentration

–O groups which are electronegative in nature. In presence of polymer, the electrons were pulled out causing deshielding, whereas because of the increased electron density shielding occurs. The shift in the aromatic protons and –NH peaks itself represents drug-polymer interaction.

With Soluplus, a slight shift in aromatic protons was observed; however, the –NH peak disappeared at all concentrations. The possible reason for such interaction can be because, majorly, Soluplus acts by micellar solubilization, but some literature also reports Soluplus interaction by hydrogen bond formation. The NMR results indicate the positive effect of polymers on the drug precipitation behavior.

Conclusion

We have demonstrated that compendial/biorelevant media and polymers (type and concentration) have distinctive influence on the supersaturation behavior of poorly soluble drugs. The precipitation tendency of both drugs was increased in presence of each other. This observation shows the importance of *in vitro* supersaturation studies for multidrug therapy, especially with hydrophobic molecules. The polymers were evaluated in terms of equilibrium solubility, droplet size, and precipitation kinetics. Soluplus was found to be the most effective precipitation inhibitor followed by Kolliphor HS15 and PVP K90. Solid

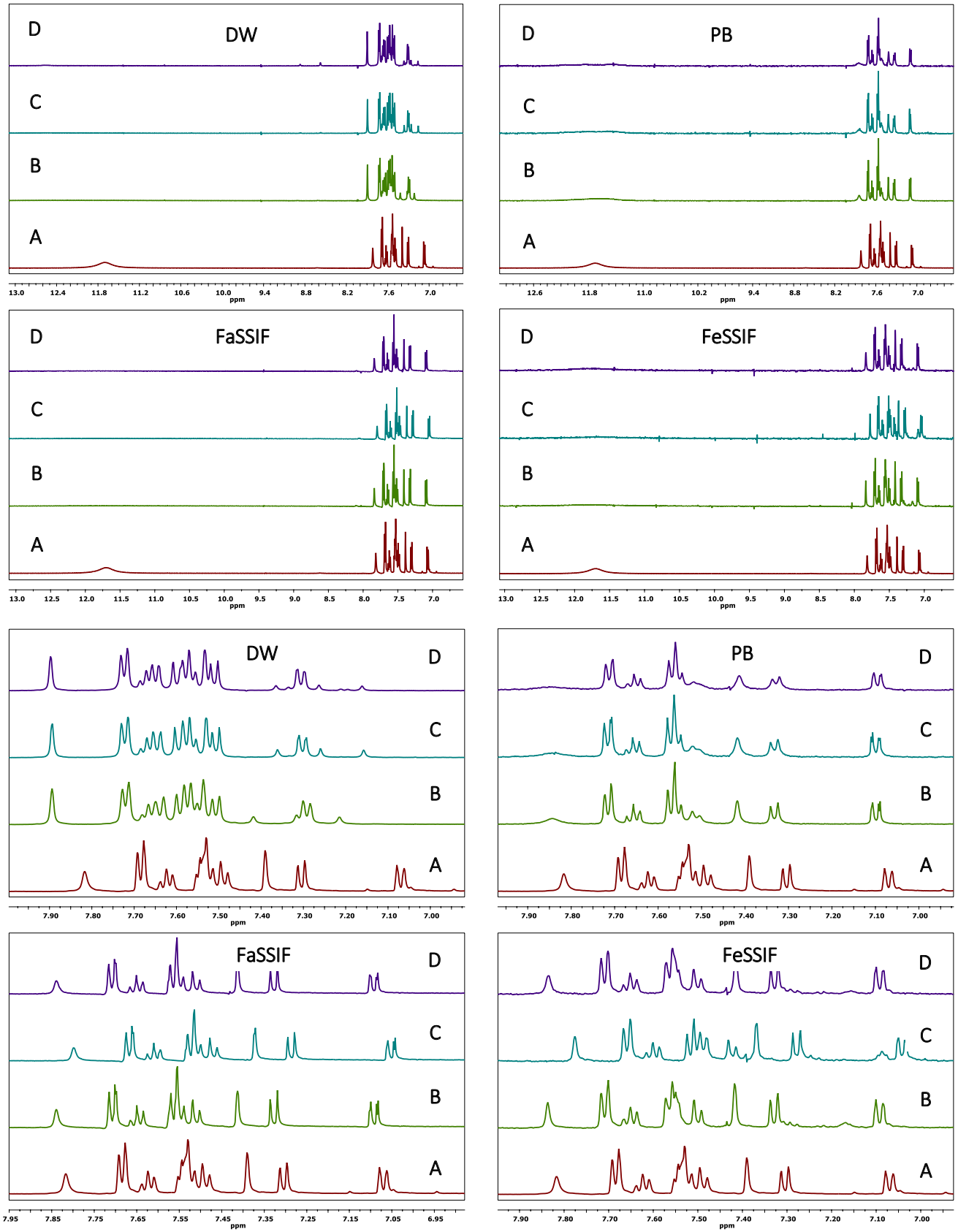

Fig. 10 NMR overlay of AMB-SOL precipitates representing –NH and aromatic protons. A represents AMB, B represents 0.05%, C represents 0.2% and D represents 1.0% w/v of Soluplus

and solution state interaction is important to understand the mechanism behind *in vitro* drug-drug and drug-polymer interplay. The interaction between drugs and polymers can differ based on their physicochemical properties. Conversion of the crystalline drug into amorphous form (DSC and PXRD) or nanodroplets (Zetasizer) can result in enhanced drug solubility. As a result of this study, Soluplus seems to be a potential stabilizer which further can be formulated into a suitable supersaturated delivery system. The study reveals that arriving at the conclusion over a single experiment may be premature, and hence multiple studies are required to select a suitable polymer for supersaturation maintenance of drugs *in vitro* and *in vivo*.

Supplementary Information The online version contains supplementary material available at https://doi.org/10.1208/s12249-022-02448-w.

Acknowledgements The authors would like to acknowledge the Director, NIPER S.A.S. Nagar, for providing the necessary facilities and infrastructure.

Author Contribution Prachi Joshi: conceptualization, data curation, formal analysis, investigation, writing—original draft, and writing—review and editing.

Abhay T Sangamwar: conceptualization, data curation, formal analysis, project administration, validation, and writing—review and editing.

Funding The authors are grateful to NIPER, SAS Nagar for providing financial support for this project.

Declarations

Conflict of Interest The authors declare no competing interests.

References

1. Prasad D, Chauhan H, Atef E. Role of molecular interactions for synergistic precipitation inhibition of poorly soluble drug in supersaturated drug–polymer–polymer ternary solution. Mol Pharmaceutics. 2016;13:756–65. https://doi.org/10.1021/acs.molpharmaceut.5b00655.
2. Guan J, Liu Q, Jin L, Xu H, Wu H, Zhang X, et al. Synergistic effect of Soluplus and hyaluronic acid on the supersaturation maintenance of lovastatin: the facilitated in vitro-in vivo performance and improved physical stability. Carbohydr Polym. 2019;222:114978. https://doi.org/10.1016/j.carbpol.2019.114978.
3. Figueirêdo CBM, Nadvorny D, de Medeiros Vieira ACQ, de Medeiros Schver GCR, Sobrinho JLS, Neto PJR, et al. Enhanced delivery of fixed-dose combination of synergistic antichagasic agents posaconazole-benznidazole based on amorphous solid dispersions. Eur J Pharm Sci. 2018;119:208–18. https://doi.org/10.1016/j.ejps.2018.04.024 (Elsevier).
4. Arca HÇ, Mosquera-Giraldo LI, Dahal D, Taylor LS, Edgar KJ. Multidrug, anti-HIV amorphous solid dispersions: nature and mechanisms of impacts of drugs on each other's solution concentrations. Mol Pharmaceutics. 2017;14:3617–27. https://doi.org/10.1021/acs.molpharmaceut.7b00203.
5. Trasi NS, Taylor LS. Thermodynamics of highly supersaturated aqueous solutions of poorly water-soluble drugs-impact of a second drug on the solution phase behavior and implications for combination products. J Pharm Sci. 2015;104:2583–93. https://doi.org/10.1002/jps.24528.
6. Trasi NS, Taylor LS. Dissolution performance of binary amorphous drug combinations–impact of a second drug on the maximum achievable supersaturation. Int J Pharm. 2015;496:282–90. https://doi.org/10.1016/j.ijpharm.2015.10.026.
7. World Health Organization Model List of Essential Medicines – 22nd List. 2021
8. Guideline: preventive chemotherapy to control soil-transmitted helminth infections in at-risk population groups. 2017
9. WHO. Schistosomiasis and soil-transmitted helminthiases: progress report, Weekly Epidemiological Record. World Health Organization; (2020) 96:585–95
10. WHO. Weekly Epidemiological Record, 2021, vol. 96, 48. Weekly Epidemiological Record. World Health Organization; 96:585–96.
11. Al Amin ASM WR. Helminthiasis. tatPearls Publishing. 2022.
12. Namwanje H, Kabatereine NB, Olsen A. Efficacy of single and double doses of albendazole and mebendazole alone and in combination in the treatment of Trichuris trichiura in school-age children in Uganda Trans R Soc Trop Med Hyg. Royal Society of Tropical Medicine and Hygiene. 2011;105:586–90. https://doi.org/10.1016/j.trstmh.2011.07.009.
13. Cowan N, Vargas M, Keiser J. In vitro and in vivo drug interaction study of two lead combinations, oxantel pamoate plus albendazole and albendazole plus mebendazole, for the treatment of soil-transmitted helminthiasis. Antimicrob Agents Chemother. 2016;60:6127–33. https://doi.org/10.1128/AAC.01217-16.
14. Keiser J, Tritten L, Adelfio R, Vargas M. Effect of combinations of marketed human anthelmintic drugs against Trichuris muris in vitro and in vivo. Parasit & Vectors. 2012;5:1–7. https://doi.org/10.1186/1756-3305-5-292.
15. Speich B, Moser W, Ali SM, Ame SM, Albonico M, Hattendorf J, et al. Efficacy and reinfection with soil-transmitted helminths 18-weeks post-treatment with albendazole-ivermectin, albendazole-mebendazole, albendazole-oxantel pamoate and mebendazole. Parasit & Vectors. 2016;9:1–10. https://doi.org/10.1186/s13071-016-1406-8.
16. Ghanbarzadeh S, Khalili A, Jouyban A, Emami S, Javadzadeh Y, Solhi M, et al. Dramatic improvement in dissolution rate of albendazole by a simple, one-step, industrially scalable technique. Res Pharm Sci. 2016;11:435. https://doi.org/10.4103/1735-5362.194868.
17. Carlert S, Åkesson P, Jerndal G, Lindfors L, Lennernäs H, Abrahamsson B. In vivo dog intestinal precipitation of mebendazole: a basic BCS class II drug. Mol Pharmaceutics. 2012;9:2903–11. https://doi.org/10.1021/mp300224h.
18. García-Rodriguez JJ, de la Torre-Iglesias PM, Vegas-Sánchez MC, Torrado-Durán S, Bolás-Fernández F, Torrado-Santiago S. Changed crystallinity of mebendazole solid dispersion: improved anthelmintic activity. Int J Pharm. 2011;403:23–8. https://doi.org/10.1016/j.ijpharm.2010.10.002.
19. Joshi P, Mallepogu P, Kaur H, Singh R, Sodhi I, Samal SK, et al. Explicating the molecular level drug-polymer interactions at the interface of supersaturated solution of the model drug: albendazole. Eur J Pharm Sci. 2021;167:106014. https://doi.org/10.1016/j.ejps.2021.106014.
20. Jantratid E, Janssen N, Reppas C, Dressman JB. Dissolution media simulating conditions in the proximal human gastrointestinal tract: an update. Pharm Res. 2008;25:1663–76. https://doi.org/10.1007/s11095-008-9569-4.
21. Sodhi I, Sangamwar AT. Microarray plate method for estimation of precipitation kinetics of celecoxib under biorelevant conditions and precipitate characterization. Mol Pharmaceutics. 2018;15:2423–36. https://doi.org/10.1021/acs.molpharmaceut.8b00267.

22. Chavan RB, Thipparaboina R, Kumar D, Shastri NR. Evaluation of the inhibitory potential of HPMC, PVP and HPC polymers on nucleation and crystal growth. RSC Adv. 2016;6:77569–76. https://doi.org/10.1080/03639045.2018.1503295.
23. Pas T, Struyf A, Vergauwen B, Van den Mooter G. Ability of gelatin and BSA to stabilize the supersaturated state of poorly soluble drugs. E Eu J Pharm Biopharm. 2018;131:211–23. https://doi.org/10.1016/j.ejpb.2018.08.003.
24. Jackson MJ, Kestur US, Hussain MA, Taylor LS. Characterization of supersaturated danazol solutions - impact of polymers on solution properties and phase transitions. Pharm Res. 2016;33:1276–88. https://doi.org/10.1007/s11095-016-1871-y.
25. Brough C, Miller DA, Keen JM, Kucera SA, Lubda D, Williams RO 3rd. Use of polyvinyl alcohol as a solubility-enhancing polymer for poorly water soluble drug delivery (part 1). AAPS PharmSciTech. 2016;17:167–79. https://doi.org/10.1208/s12249-015-0458-y.
26. Shi N-Q, Lai H-W, Zhang Y, Feng B, Xiao X, Zhang H-M, et al. On the inherent properties of Soluplus and its application in ibuprofen solid dispersions generated by microwave-quench cooling technology. Pharm Dev Technol. 2018;23:573–86. https://doi.org/10.1080/10837450.2016.1256409.
27. Ducheyne P, Healy KE, Hutmacher DW, Grainger DW, Kirkpatrick CJ. Comprehensive biomaterials [Internet]. Elsevier Science; 2015.
28. Glöckner G. Gradient polymer chromatography: liquid chromatography. In: Wilson ID, editor. Encyclopedia of Separation Science. Oxford: Academic Press; 2000. p. 2975–84. https://doi.org/10.1016/B0-12-226770-2/01851-2
29. Joshi P, Sangamwar AT. Stabilizing supersaturated drug-delivery system through mechanism of nucleation and crystal growth inhibition of drugs. Ther Deliv. 2018;9:873–85. https://doi.org/10.4155/tde-2018-0031.
30. Taylor LS, Zografi G. Spectroscopic characterization of interactions between PVP and indomethacin in amorphous molecular dispersions. Pharm Res. 1997;14:1691–8. https://doi.org/10.1023/a:1012167410376.
31. Dai W-G, Dong LC, Li S, Deng Z. Combination of Pluronic/Vitamin E TPGS as a potential inhibitor of drug precipitation. Int J Pharm. 2008;355:31–7. https://doi.org/10.1016/j.ijpharm.2007.12.015.
32. Brits M, Liebenberg W, de Villiers MM. Characterization of polymorph transformations that decrease the stability of tablets containing the WHO essential drug mebendazole. Pharm Sci. 2010;99:1138–51. https://doi.org/10.1002/jps.21899.
33. Raval MK, Vaghela PD, Vachhani AN, Sheth NR. Role of excipients in the crystallization of albendazole. Adv Powder Technol. 2015;26:1102–15. https://doi.org/10.1016/j.apt.2015.05.006.
34. Koradia KD, Parikh RH, Koradia HD. Albendazole nanocrystals: optimization, spectroscopic, thermal and anthelmintic studies. J Drug Deliv Sci Technol. 2018;43:369–78. https://doi.org/10.1016/j.jddst.2017.11.003.
35. Aboul-Enein HY, Bunaciu AA, Fleschin S. Analysis of mebendazole polymorphs by Fourier transform IR spectrometry using chemometric methods. Biopolymers. 2002;67:56–60. https://doi.org/10.1002/bip.10041.

Publisher's Note Springer Nature remains neutral with regard to jurisdictional claims in published maps and institutional affiliations.

Springer Nature or its licensor (e.g. a society or other partner) holds exclusive rights to this article under a publishing agreement with the author(s) or other rightsholder(s); author self-archiving of the accepted manuscript version of this article is solely governed by the terms of such publishing agreement and applicable law.

molecular pharmaceutics

Article

Cite This: Mol. Pharmaceutics 2018, 15, 2423−2436

Microarray Plate Method for Estimation of Precipitation Kinetics of Celecoxib under Biorelevant Conditions and Precipitate Characterization

Ikjot Sodhi and Abhay T. Sangamwar*

Department of Pharmaceutics, National Institute of Pharmaceutical Education and Research, Sector-67, S.A.S. Nagar, 160062, Punjab, India

Supporting Information

ABSTRACT: Study methodologies of supersaturated state are fast developing as pharmaceutical industry is adopting supersaturating drug delivery systems (SDDS) to overcome the solubility issue of drugs. The "parachute" of sobriquet "spring-and-parachute", which indicates delayed or slowed intraluminal precipitation of drug from SDDS, is of immense importance to formulation scientists since optimal attainment of "parachute" governs the success of SDDS in stabilizing supersaturated state that ensues in enhancement of bioavailability. The studies carried out so far for precipitation assessments have ignored the stochastic nature of nucleation and lack absolute mathematical approach. In the current study, the supersaturated state has been studied in a quantitative manner through microarray plate method with application of the classical nucleation theory (CNT) equation for determination of precipitation kinetics. This microarray plate method is an attempt to pursue the principle of miniaturization in supersaturation assays and involves comprehensive measurements that allows for accounting of the stochastic nature of nucleation. Overcoming the drawbacks of reproducibility and greater material requirement of existing methods, this study aims to quantify the rate of *in vivo* precipitation through understanding of precipitation profile of model drug, celecoxib, in biorelevant media. Quantification of nucleation rates was made through CNT using tailored criteria and visually represented through temporal precipitation distribution (TPD) plots. Supersaturation stability was also compared through metastable zone width (MSZW). Optical microscopy helped in visualizing the dynamics of precipitation, while solid state characterization assisted in understanding the nature of obtained precipitates. This study identified the short-lived supersaturation of celecoxib and its tendency to precipitate under fasted conditions, which can be correlated with *in vivo* behavior for formulation design.

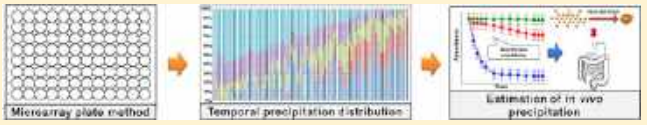

KEYWORDS: *precipitation kinetics, microarray plate, biorelevant media, spectrophotometry, supersaturation assay*

Downloaded via NIPER MOHALI on August 22, 2023 at 09:15:54 (UTC).
See https://pubs.acs.org/sharingguidelines for options on how to legitimately share published articles.

INTRODUCTION

Novel formulation approaches are sought to overcome the issue of low bioavailability that ensues from poor aqueous solubility of drugs. With nearly 40% of marketed molecules and 90% of molecules in development pipeline classed as poorly soluble, technologies and excipients used in formulation of such drugs have gained huge business prospects.[1] Stepping ahead of the fast disintegrating approaches for faster release of drugs,[2] formulation approaches today have become more complicated and tedious. Supersaturating drug delivery systems (SDDS) have already started dominating the research as well as commercial interests of pharmaceutical community. SDDS is a collective term for formulation approaches that target to overcome solubility issues through generation of intraluminal concentration of drugs beyond their thermodynamic solubility. These approaches include amorphous solid dispersions (ASDs), cocrystals, nanoparticles, self-emulsifying drug delivery systems (SEDDS), coground mixtures, formulation with inorganic carriers like mesoporous silica, prodrugs, and salt formation, which have been commercially successful in enhancing the bioavailability of drugs.[3] The *modus operandi* of SDDS has been explained through "spring-and-parachute" effect where the "spring" is rapid solubilization of a drug in media with the drug attaining supersaturated state, while the "parachute" signifies stabilization of the metastable supersaturated state through delaying or inhibiting the drug precipitation process. Targeting this formulation approach involves modification of the solid state of the drug through crystal engineering or use of high energy/rapidly dissolving solids along with the use of precipitation inhibiting excipients making it an alpha strategy for formulation.[3−5] Advantage attributed by SDDS roots to ensuing high intraluminal chemical potential of drug molecule that results in its increased diffusion tendency and thereby higher permeability across the biological membranes in accordance with Fick's law of diffusion.[6] This phenomenon is different from formulation techniques like micellar solubilization, cosolvents, and cyclodextrins among others that enhance the apparent solubility of a compound without increasing its chemical potential. Distinction of the two

Received: March 14, 2018
Revised: May 3, 2018
Accepted: May 10, 2018
Published: May 10, 2018

© 2018 American Chemical Society

DOI: 10.1021/acs.molpharmaceut.8b00267
Mol. Pharmaceutics 2018, 15, 2423−2436

phenomena has gained recognition as the latter mechanism does not increase the permeation of drug across biological membranes owing to decreased availability of free drug in solubilizing media.[7,8] SDDS like ASDs, SEDDS, and formulation with mesoporous silica carriers have demonstrated enhancement in solubility of drug molecules along with increased intestinal permeability.[7,9−13]

While evaluation of high energy solids has advanced with sophisticated techniques and methodologies like differential scanning calorimetry (DSC), powder X-ray diffraction (PXRD), Fourier transformed-infrared (FTIR) spectroscopy, and solid-state nuclear magnetic resonance (ssNMR), evaluation of supersaturated state stability is still imprecise and subject to variability. Until now, a general supersaturation assay involves generation of supersaturation through either solvent shift or pH change followed by capturing of precipitation process through either direct monitoring of precipitated particles by turbidimetry, nephelometry,[14] focused beam reflectance measurement (FBRM),[15,16] or dynamic light scattering (DLS)[17,18] or indirectly through measurement of the decline of solute concentration in media through UV spectrophotometry[19,20] or HPLC analysis.[21]

Due to its versatility, lesser labor requirement, and ability to control the rate and extent of supersaturation generation, solvent shift method has been widely used in the supersaturation assessment of various drugs. This process involves generation of supersaturation by the addition of a concentrated solution of drug in medium (usually aqueous) in which the drug has poor solubility. The method has been used to detect liquid−liquid phase separation (LLPS) and to determine precipitation inhibition potential of various excipients. Solvent shift method is mostly adopted for supersaturation assessment without regard to formulation consideration. Concentrated solutions (1−2 mL) of varying concentration range maybe introduced to test media of volume 25 to 500 mL for precipitation observation. The introduction of drug at controlled rate can be assisted through the use of a syringe pump.[20−27] Majorly, these supersaturation assays aim to compare the efficacy of polymers in preserving the metastable supersaturated state. Warren et al. described three types of desupersaturation curves obtained in the presence of polymers with Type A being a desirable profile for a good precipitation inhibitor, while Type C is the least preferred one.[14] While the method is less labor intensive, methods used in various laboratories have the drawbacks of being bulky and giving only qualitative or majorly semiquantitative results. Although attempts are made to apply the data into classical nucleation theory (CNT) equations for quantification of nucleation rates, however, those are not based upon a comprehensive number of measurements.[26] The lengthy measurements allow fewer replicates for any reading, and variability remains a problem owing to variations in concentration of stock solution, rate of addition into media, volume of media and stock solution, rate of agitation, and subjection to intermittent withdrawal of aliquots for analysis. Due to the sensitivity of the precipitation process to various factors like hydrodynamics, the presence of impurities, temperature, supersaturation index, and complex gastrointestinal environment, it is challenging to develop a method that would assess biorelevant precipitation kinetics on an absolute basis. Adding to variability is the stochastic nature of nucleation phenomenon. Nucleation has been widely accepted as a stochastic process due to observed variations in results even in identical experimental conditions. Hence, a large set of replicates is required to account for the variability arising from its stochastic nature.

Microarray plates have potential of overcoming disadvantages of bulky supersaturation assays and decease analysis time by increasing replicates and lowering sample size. This tool has already found its niche in the domain of crystallization as a screening tool with applications varying from selecting conditions suitable for crystallization of macromolecules[28] to screening of excipients as precipitation inhibitors for amorphous solid dispersion.[29] Dai et al. demonstrated the use of a 96-well plate to assess the precipitation kinetics of three liquid formulations of a new molecular entity (NME) with different precipitation kinetics in biorelevant media through analysis by high performance liquid chromatography (HPLC).[30] Microplate assays combining quantitative analysis of supernatant with turbidimetry have also been demonstrated as a screening tool to rank-order supersaturation limits of early drug candidates.[31] Microplate based assays are hence gaining recognition in the domain of assessment of supersaturation stabilization and precipitation kinetics.

Attempts are made to map metastable zone width (MSZW) and measure induction times from the desupersaturation profile of drugs as a measure of supersaturation stability. MSZW is a visual representation of the degree of stabilization of the supersaturated state under a specific set of conditions and is demarcated as the zone between the solubility curve and the metastable limit curve. MSZW is routinely used in batch crystallization operations where MSZW mediated understanding of the precipitation behavior of solute helps in carrying out controlled precipitation to get crystals of narrow particle size distribution.[32−34] While the purpose of evaluating the metastable supersaturated state for batch crystallization processes is for executing controlled crystallization, the objective of the same under biorelevant conditions is to prevent it. SDDS generate gastrointestinal concentrations of drug much higher than its thermodynamic solubility, which in turn fuels its recrystallization, thereby limiting the solubility advantage. Assessment of the precipitation profile of a drug under biorelevant conditions becomes necessary to understand the fate of drug and its impact on bioavailability. Quantitative precipitation data can be applied in physiologically based pharmacokinetic (PBPK) models for establishing *in vitro−in vivo−in silico* (IVIVIS) correlations that can be utilized for a model-informed development of SDDS. Determination of precipitation kinetics becomes imperative for BCS class II and IV drugs whose bioavailability is limited by poor dissolution and precipitation of dissolved drug. Commercially available PBPK platforms integrate the consideration of precipitation kinetics of drugs for estimation of "absorbable" dose. GastroPlus uses mean precipitation time and pH-dependent precipitation profiles as inputs for precipitation data. Hens et al. have used the *in silico* dissolution and precipitation data of posaconazole using Simcyp In Vitro data Analysis (SIVA) toolkit for estimation of its pharmacokinetics using Simcyp population simulator.[35] As the regulatory and commercial interests are increasingly growing toward model informed drug development (MIDD) for reduced failures in drug development, integration of precipitation kinetics with PBPK models can be directed toward guided selection of excipients for formulation through assessment of impact on bioavailability.

The current study aimed at understanding the precipitation behavior of a model drug, celecoxib (CEL), under biorelevant

DOI: 10.1021/acs.molpharmaceut.8b00267
Mol. Pharmaceutics 2018, 15, 2423−2436

conditions. The precipitation kinetics was assessed through a microarray plate method involving a comprehensive number of measurements and application of CNT for assessment of nucleation rates. Further, precipitation kinetics was also studied in certain components of biorelevant media in order to identify the factors unfavorable for supersaturation of CEL. The study also introduces two-dimensional plots termed "temporal precipitation distribution" diagrams that represent the degree of precipitation in different time intervals. Solid state characterization and optical microscopy were performed to assess the nature of drug reprecipitated under biorelevant conditions.

THEORY

Nucleation is widely studied as a kinetic process, although the mechanism itself remains an unsolved riddle. Nucleation time, as a measure of nucleation rate, is difficult to detect as the microscopic nucleus are beyond the detection limits of the naked eye and currently used techniques. Induction time is widely adopted instead, which measures the time from supersaturation generation at which the first formed nucleus grows enough to be detected. Nucleus formation, a stochastic process, continues occurring at the free energy levels of the supersaturated solution. Formation of a nucleus is a rare event described as a Poisson process where the number of nuclei formed following Poisson distribution (eq 1).[36,37]

$$N(t) = 1 - \exp\left(-\int_0^t k(t)\mathrm{d}t\right) \tag{1}$$

where $N(t)$ stands for the fraction of samples that showed formation of first stable nucleus within time t; $k(t)$ is the rate constant that, when multiplied by finite interval of time, gives the probability of occurrence of the Poisson event in that time interval. Probability distributions of induction times, t_{ind}, have been used for calculation of nucleation rates.

Using eq 1, the induction times so estimated can be expressed as a Poisson process and converted into a cumulative probability distribution, $N(t)$.

$$N(t) = 1 - \exp(-JVt) \tag{2}$$

where J is nucleation rate, V is volume of media, and t is induction time. Fitting eq 2 with the experimentally determined probability leads to a value for the nucleation rate (J).[36]

According to classical nucleation theory (CNT), free energy for nucleation is the interplay between two terms of radius (r) raised to exponents representing surface term and volume term, having opposite impact on free energy for nucleus formation.[38]

$$\Delta G = \frac{-4\pi r^3}{3\nu} KT \ln S + 4\pi r^2 \sigma \tag{3}$$

where the first term represents the bulk free energy contribution at temperature T with K as the Boltzmann constant in a cluster of $\frac{4\pi r^3}{3\nu}$ number of molecules with each molecule having radius r and volume ν at a supersaturation index of S. σ is the interfacial energy between the media and the newly formed surface.

In order to find the critical nucleus radius (r^*), eq 3 is differentiated with respect to r. This gives the critical radius r^* as

$$r^* = \frac{2\sigma}{KT} \ln S \tag{4}$$

and the barrier to nucleation as

$$\Delta G^* = \frac{16\pi\sigma^3\nu^2}{3K^2T^2(\ln S)^2} \tag{5}$$

Using this free energy, nucleation rate, J, can be expressed as an Arrhenius equation giving the final expression for J as[38]

$$J = A \exp\left(-\frac{16\pi\sigma^3\nu^2}{3K^3T^3(\ln S)^2}\right) \tag{6}$$

Taking the pre-exponential and exponential constants as A and B, the nucleation rate at supersaturation ratio S can be expressed as[36]

$$J(S) = AS \exp\left(-\frac{B}{\ln^2 S}\right) \tag{7}$$

where A and B are kinetic and thermodynamic parameters, respectively.

CNT has been successfully applied for giving a quantitative description of critical supersaturation and nucleation rates in some systems like water. However, it failed in its purpose of a quantitative description for complex systems leading to limitation of its predictive ability. Also, CNT does not explain the decrease in nucleation barrier at higher supersaturation.[38]

A nonclassical approach to explain crystallization is the density functional theory (DFT) that considers the factor of critical spherical density instead of radius as the driving factor for nucleus formation. It is based on the assumption that the density of the nucleus is different from that of the media as well as of the new phase. When a cluster reaches a critical density profile ρ, growth of a new phase becomes favorable. Adopting the pre-exponential kinetic factor A from CNT, DFT estimates the rate of formation of critical nucleus (in per unit volume) as

$$J_{DFT} = A \exp^{-\Delta\Omega_{DFT}/K_BT} \tag{8}$$

The free energy term $\Delta\Omega_{DFT}$ is calculated through density functional methods using intermolecular potentials of the systems approximated through hard-sphere perturbation theory. The consideration of supersaturation levels is made through the dependency of term $\Delta\Omega_{DFT}$ on the chemical potential of a molecule.[38]

Model Drug. Celecoxib (CEL; Figure 1), a BCS class II drug, was chosen as the model drug for this study.

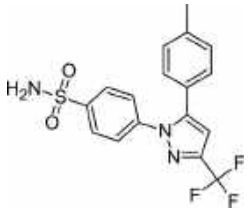

Figure 1. Structure of CEL.

Pharmacokinetic study on dogs showed CEL has higher bioavailability from solution (64−88%) than from capsule (22−40%) and identified dissolution as the rate-limiting factor in its absorption.[39]

EXPERIMENTAL SECTION

Materials. Celecoxib was procured from Dr. Reddy's Laboratories as gift sample and was used as received. Sodium

DOI: 10.1021/acs.molpharmaceut.8b00267
Mol. Pharmaceutics 2018, 15, 2423−2436

taurocholate hydrate was purchased from Alfa Aesar, while lecithin (grade S75) was obtained as a gift sample from Lipoid GmBH. All other chemicals used in this study were of laboratory grade. Water (resistivity 18.25 MΩ·cm) purified from a water purification system (Millipore Synergy UV system) was used.

Methods. *Preparation of Media.* Biorelevant media fasted state simulated gastric fluid (FaSSGF), fasted state simulated intestinal fluid version 2 (FaSSIF-v2), and fed-state simulated intestinal fluid version-2 (FeSSIF-v2) were prepared with compositions as described by Dressman et al.[40] Fed state simulated gastric fluid (FeSSGF) was found unsuitable for a spectrophotometric mode of detection due to associated properties of creaming and turbidity. Buffered nutrition cocktail (BNC) having three basic components of food (carbohydrates, proteins, and fats) and composition described in Table 1 was prepared and used as a replacement of FeSSGF. The media were passed through cellulose filter papers (Whatman grade 0903; pore size 11 μm) before use.

Table 1. Composition and Preparation of Buffered Nutrition Cocktail (BNC)[a]

composition	quantity
deionized water	100 mL
starch	500 mg
dextrose	500 mg
egg albumin	500 mg
soyabean oil	200 μL
glyceryl monooleate (GMO)	200 mg
sodium chloride	700 mg
sodium acetate	102.7 mg
acetic acid	100 mg (87 μL)
properties	**quantity**
pH	5.0

[a]Procedure: All components except acetic acid, soyabean oil, and GMO were dissolved in deionized water. Soyabean oil and GMO were dissolved in diethyl ether and then added to the mixture. Diethyl ether was evaporated over rota vapor at 49 bar and 37 °C for an hour. Acetic acid was added and pH adjusted to 5 followed by filtration through Whatman Filter Paper (pore size: 11 μm).

Solubility Studies. Equilibrium solubility of CEL was determined in different media through the shake flask method by equilibrating water, FaSSGF, FaSSIF-v2, BNC, and FeSSIF-v2 with an excess of CEL in a shaker water bath maintained at 37 °C and 60 rpm for 24 h. Blanks comprised portions of media subject to same conditions without adding CEL. In order to remove solid CEL, samples were transferred to microcentrifuge tubes and centrifuged (Spinwin microcentrifuge, Tarsons, India) at 5000 rpm for 10 min. The separated supernatant was diluted four times for FaSSIF-v2 and five times for FeSSIF-v2 and BNC samples with methanol to ensure complete solubilization of micelles. Supernatants from FaSSGF and water were used without dilution. Aliquots of prepared supernatants were subject to quantification by HPLC analysis.

Analytical Method. The analytical method of CEL was developed on a Shimadzu HPLC system using a Inertsil ODS-3V column (4.6 mm × 300 mm, 5 μm) coupled to a PDA detector (Shimadzu SPD-M10A). Measurements were performed at a flow rate of 1.0 mL/min with isocratic flow of acetonitrile and aqua (pH 3.5) in a ratio of 70:30. The injection volume was 20 μL.

Osmolality Measurement. The osmolality measurements were made using vapor pressure osmometer (Vapro Vapor Pressure Osmometer Model 5520, Wescor Inc., USA). The instrument was first allowed to equilibrate for half hour followed by calibration using a calibration standard (10 μL) of 290 mmol/kg standard in normal mode. Osmolality readings of samples from FaSSGF, FaSSIF-v2, BNC, and FeSSIF-v2 were taken.

Precipitation Kinetics. Precipitation kinetics assessment was carried out in a microarray plate (polystyrene 96-well plate) with spectrophotometric determination of absorbance using SpectraMax M2^e Multidetection Reader integrated with SoftMax Pro 6.2.1. (Build number: 186682), both provided by Molecular Devices. Adopting solvent-shift method for supersaturation generation, three concentrations of methanolic stock solutions of CEL were prepared viz. 5, 7, and 10 mg/mL to understand the precipitation kinetics at different supersaturation index (SSI). SSI is calculated as the ratio of concentration of CEL in media generated from spiking of an amount of CEL (C_{amt}) to its equilibrium solubility in media (C_{eq}) as represented in eq 9.

$$\mathrm{SSI} = \frac{C_{amt}}{C_{eq}} \tag{9}$$

For every assay, media was prewarmed at 37 °C followed by transfer of 300 μL in each of 88 wells. CEL stock solution (10 μL) of a single concentration was spiked in each well using an Eppendorf multichannel pipet. The plate was immediately subject to absorbance measurements at wavelengths of minimal interference (300 nm for FaSSGF, FaSSIF-v2, and BNC and 310 nm for FeSSIF-v2). Temperature was set at 37 °C, and intermittent agitation was included in protocol by setting initial shaking for 3 s and shaking between reads for 2 s. In order to alleviate interference from scattering due to formed precipitates, Savitzky-Golay 5-point smoothing algorithm was applied using Microcal Orgin 6.0 statistical software (Microcal Software, Inc., Northhampton, USA).

Compositional Effect on Supersaturation. In order to understand the effect of components of biorelevant media on the supersaturation behavior of CEL, precipitation kinetics was assessed individually in water, acidified aqua (at gastric pH 1.6), gastric and intestinal concentration of lecithin (20 μM and 0.2 mM) at pH 6.8, sodium taurocholate (80 μM and 3 mM) at pH 6.8, and pepsin at pH 1.6. A CEL stock solution of 4 mg/mL was spiked (10 μL) using an Eppendorf multichannel pipet in 88 wells containing media (300 μL). Absorbance measurements were taken at 300 nm for an hour.

In Silico Assessment. Structure of CEL was retrieved from Zinc12 database (Irwin and Shoichet Laboratories, University of California, San Francisco) and given as input to ADMET Predictor (version 8.1.0.11; license code 23; Simulations Plus, Lancaster, USA) for calculation of its physicochemical properties.

Solid State Characterization. Precipitates from each media obtained using the supersaturation level corresponding to C3 were filtered and pressed between the folds of cellulose filter paper (Whatman grade 0903) followed by drying in an oven at 40 °C for at least 12 h and then stored with desiccators until further analysis. For understanding the polymorphic form of CEL in precipitates, PXRD patterns were obtained at room temperature using Bruker's model D8 Advance Diffractometer (Karlsruhe, West Germany) equipped with a 2θ compensating

DOI: 10.1021/acs.molpharmaceut.8b00267
Mol. Pharmaceutics 2018, 15, 2423−2436

slit, using Cu Kα radiation (1.54 Å) at 40 kV and 40 mA passing through nickel filter with divergence slit (0.5°), antiscattering slit (0.5°), and receiving slit (0.1 mm). Samples were mounted on a zero-background sample holder and scanned continuously over an angular range of 5−40° 2θ at a step size of 0.01° and scan rate of 1 s/step. Obtained diffractograms were analyzed with DIFFRACplus EVA (ver. 9.0) diffraction software.

For determination of a polymorphic form of CEL in precipitates obtained from each media, melting endotherms of each precipitate were studied through DSC performed using DSC 821e (Mettler-Toledo GmbH, Schwerzenbach, Switzerland) operating with STARe software version 5.1. Calibration of the system for temperature and heat flow was performed using high purity indium standard. Sample (nearly accurately 3−5 mg) was weighed into a crimped aluminum pan with a Mettler Toledo balance, while the reference pan was left empty. Both were cold-sealed and placed in a sample cell prior to being purged with dry nitrogen at a flow of 40 mL/min. Heating was carried out at the rate of 20 °C per minute from ambient temperature to 200 °C.

Morphological examination of precipitates at ambient temperature was made through scanning electron microscope (SEM) imaging. The powder samples were mounted onto a steel stage using double sided adhesive tape and sputter coated with gold−palladium using ion sputter (E-1010, Hitachi Ltd., Tokyo, Japan) and examined under different magnification by SEM (S-3400N, Hitachi, Japan) operating at an excitation voltage of 25 kV.

Optical Microscopy. In order to observe the generation of any intermediate polymorph, optical microscopy was carried out along with the application of polarized light for the observation of birefringence using Leica DMLP polarized microscope (Leica Microsystems Wetzlar GmbH, Wetzlar, Germany) equipped with Leica JVC digital camera integrated with Leica IM 50 (version 1.20) software for visualization through digital monitors. Before observation of precipitation, pure CEL was used on a concavity slide to set the focus of the microscope through a 10× objective. Media (20 μL) was added to the clean concavity slide well and placed under a microscope. A large quantity of media does not evaporate quickly for the time of observation and is convenient for appropriate spiking with methanolic stock solution. The well of the concavity slide restrained fluid and prevented its mobility. Then 2−3 μL of stock solution (5 mg/mL) was added to the media and stirred using a pipet tip. Observations were made for the appearance of precipitates and associated birefringence in both optical and birefringence mode through polarized light.

RESULTS AND DISCUSSIONS

Effect of SSI on Precipitation. Solubilities of CEL in media were determined as 1.0 μg/mL in FaSSGF, 11.52 μg/mL in FaSSIF-v2, 7.6 μg/mL in BNC, and 65.4 μg/mL in FeSSIF-v2. Using the volumes of gastric and intestinal media generalized for dissolution tests,[41] solubilization of a single 200 mg dose of CEL would generate gastric and intestinal CEL levels whose SSI values have been calculated as stated in Table 2. The supersaturation indices of CEL used in the current study (Table 2) are of the order encountered during intraluminal solubilization of CEL.

Temporal precipitation distribution (TPD) diagrams, developed as a comparative representation of the degree of precipitation in all samples of a media scaled with respect to time (Figure 2A−C) were plotted for precipitation observed in 88 samples of precipitation assay in FaSSGF at each supersaturation level, which showed the dominance of the blue region, indicating maximum precipitation in the first quarter-hour. An irregular distribution pattern was observed in later time zones for C1, while C2 showed nearly proportional precipitation in different demarcated time spans acting in accordance with exponential desupersaturation. A varying precipitation distribution was observed for a second quarter-hour (red region) for C3. Analysis of absorbance data (Figure 2D) showed precipitation being rapid at all levels with nearly 20−25% of the drug precipitating in the first 2.5 min. Hence, the application of the concept of induction time or $t_{10\%}$ was difficult. Precipitation was discernibly triphasic for C1 with rapid decline in absorbance in the first 10 min followed by a phase of negligible decrease forming a plateau for the next 10 min that was followed by a third stage of exponential decrease. In C2, the latter two stages seem to merge, thereby showing an exponential decrease in absorbance. In C3, precipitation was two-staged with an initial rapid decline in 20 min followed by a slow but steady decrease in absorbance. Also, the absorbance level at the trough in C3 was higher than the trough absorbance levels of C1 and C2 for the observed time. To account for this midway stabilization of the supersaturation, a tailored criterion was adopted to calculate the nucleation rates that seeked at least two-third decrease in absorbance in more than 90% of the samples. The earliest time point fulfilling this criterion was taken for calculating the nucleation time. This criterion might include a greater degree of crystal growth time but is not much different from the conventionally adopted parameter of induction time in view of the fact that induction time also includes some degree of crystal growth time in addition to the nucleation time. This criterion was fulfilled in 82 of 88 samples individually for C1 showing two-third precipitation at 45 min, C2 at 30 min, and C3 at 20 min. The fraction of positive results obtained, $N(t) = 82/88 = 0.9318$, was used in eq 2 to calculate the nucleation rate. The nucleation rates were 192.5, 288.7, and 346.5 nuclei/L/min at C1, C2, and C3, respectively. In compliance with classical nucleation theory, plots between nucleation rate and supersaturation index and between ln J and $\ln^{-2}$ S were linear with r^2 values of 0.9914 and 0.9995 (Figure 2E,F).

Precipitation was rapid at all supersaturation levels in FaSSIF-v2. The absence of cyan and orange colors from the TPD plots (Figure 3A−C) indicates complete precipitation in all samples in 1 h with the maximum precipitation (nearly 90%) occurring in the first quarter at all supersaturation indices indicated by the dominance of blue regions. The slopes of desupersaturation (Figure 3D) can be described exponential for C1 and monophasic linear for C2 and C3. The trough level absorbance remained nearly constant at all supersaturation levels. Different time points were checked at which the estimation criteria got fulfilled. Eighty-six samples of C1, 84

Table 2. Supersaturation Indices Employed in Different Media

stock solution (μL)	label	supersaturation index			
		FaSSGF	FaSSIF-v2	BNC	FeSSIF-v2
5	C1	160.8	14.0009	21.152829	2.4681
7	C2	225.2	19.60125	29.613961	3.45534
10	C3	321.6	28.00179	42.305658	4.9362

DOI: 10.1021/acs.molpharmaceut.8b00267
Mol. Pharmaceutics 2018, 15, 2423−2436

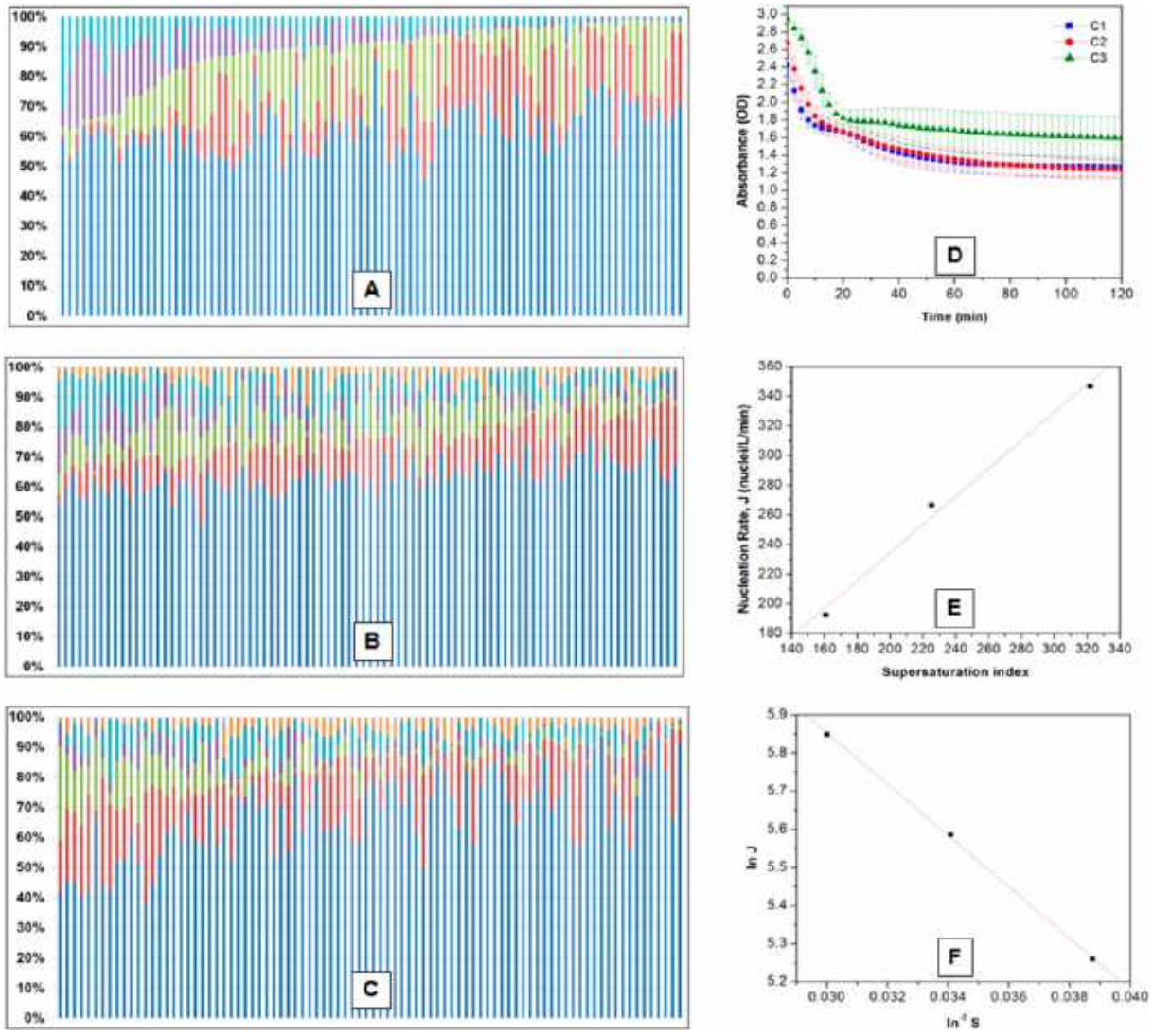

Figure 2. Temporal precipitation distribution (TPD) diagrams in FaSSGF of 88 samples each at three supersaturation indices (A) C1, (B) C2, and (C) C3 depicting the time-wise percentage of precipitation; dark blue for 0−15 min, red for 15−30 min, green for 30−45 min, purple for 45−60 min, cyan for 60−120 min, orange for 120−180 min, and light blue for 180−240 min. (D) Mean desupersaturation plots of C1, C2, and C3 in FaSSGF. (E) Plot of nucleation rate J at different supersaturation indices. (F) Plot of ln J and $\ln^{-2} S$.

samples of C2, and 86 samples of C3 of the total 88 fulfilled the criteria at 10, 5, and 5 min, respectively. With this, the nucleation rates were calculated as 1220.7, 1994.2, and 2441.4 nuclei/L/min. Nucleation rate showed linear relation with supersaturation levels (r^2 = 0.9298) along with linearity in the plot between ln J and $\ln^{-2} S$ (r^2 = 0.9769)) in compliance with CNT (Figure 3E,F).

In BNC, TPD plots (Figure 4A−C) showed varied patterns at different supersaturation indices. TPD at C1 showed that 50−60% of precipitation occurred in a majority of samples in the first quarter-hour with few samples showing variations in the range between 24 and 100%. Majority of the samples showed proportionate precipitation in the next two quarter-hours, while some samples did not show any precipitation as is reflected by the absence or negligible red and green bars. In C2, precipitation was mostly extended to the second and third quarters in a majority of the samples. Induction time can be visualized by the absence of blue bars in many samples. Cyan bars, spanning a linear precipitation range, show varying precipitation behavior in samples until the second hour. The pattern of precipitation in C3 was more regular with linear precipitation distribution at all quarters when arranged in increasing order.

C1 showed exponential decline in absorbance values until attainment of the floor value in 35−40 min followed by a steady increase in absorbance (Figure 4D). This behavior indicates the changing chemical potential, which is the driving factor of precipitation as well as the dissolution. No or little redissolution phase was observed in samples of C2 and C3, which indicated the chemical potential of CEL being large enough for unidirectional precipitation to be observed. C2 showed maintenance of supersaturation for some time followed by a linear discernible decrease in absorbance. C3 showed precipitation in two stages with an initial abrupt decline in absorbance followed by maintenance of supersaturation that gave way to a steady decline in the second stage. The stable phase of supersaturation, comparable to induction time, lasted for around 20 min in both the cases, but the phase of decline lasted longer in C3 (second stage) as compared to C2. The

DOI: 10.1021/acs.molpharmaceut.8b00267
Mol. Pharmaceutics 2018, 15, 2423−2436

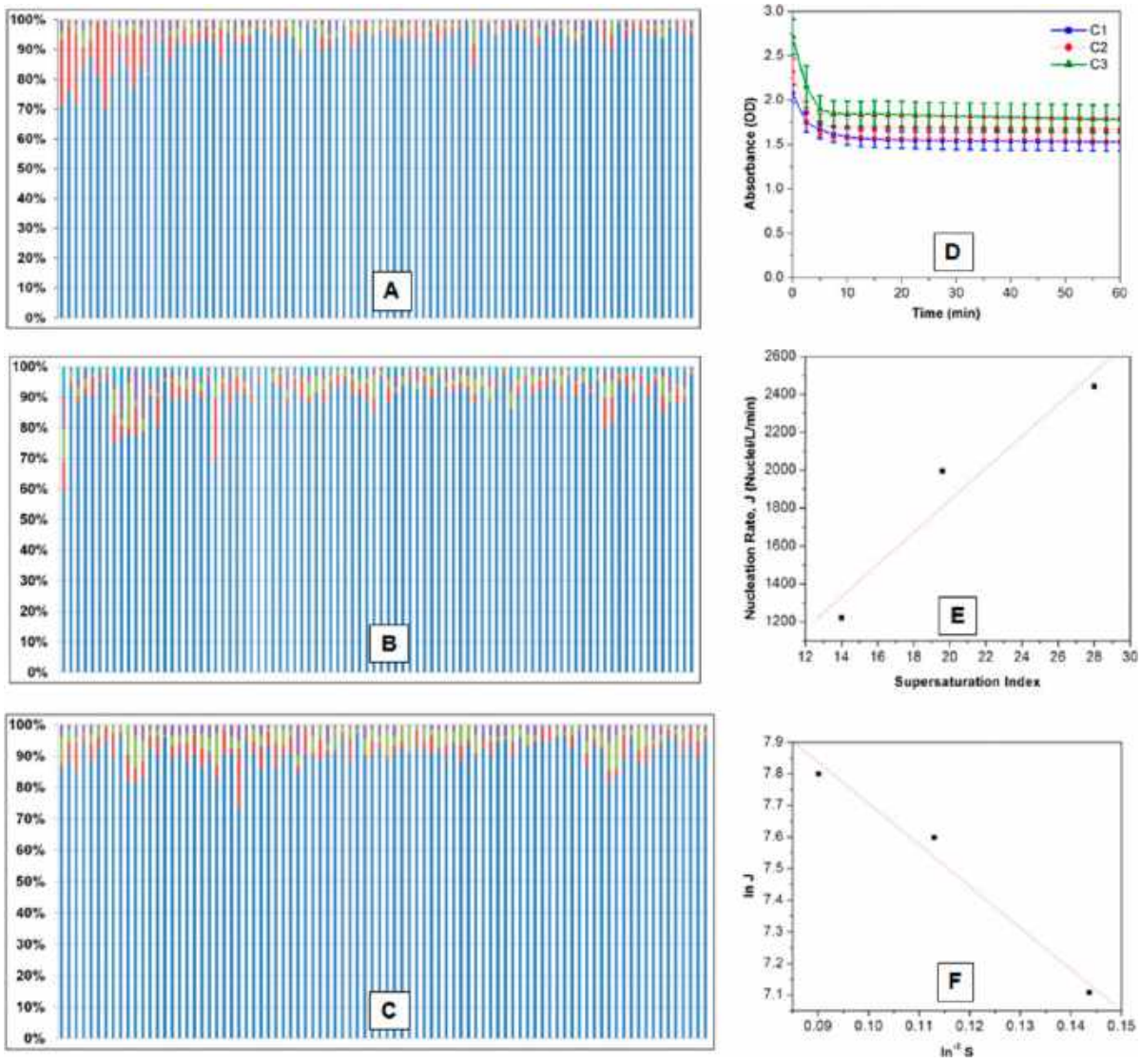

Figure 3. TPD diagrams in FaSSIF-v2 of 88 samples each at three supersaturation indices (A) C1, (B) C2, and (C) C3 depicting the time-wise percentage of precipitation; dark blue for 0−15 min, red for 15−30 min, green for 30−45 min, purple for 45−60 min, cyan for 60−120 min, orange for 120−180 min, and light blue for 180−240 min. (D) Mean desupersaturation plots of C1, C2, and C3 in FaSSIF-v2. (E) Plot of nucleation rate J at different supersaturation indices. (F) Plot of ln J and $\ln^{-2} S$.

degree of decrease in absorbance in C2 was little as compared to C3.

Nucleation rates were calculated at the earliest time points when more than 70% of samples showed 90% decrease in absorbance. Due to redissolution of compound in samples of C1 at different time points as is reflected by an increase in absorbance, it was difficult to seek the benchmark decrease in absorbance in all samples at a single time point. This criterion was fulfilled at 42.5, 80, and 65 min by 64, 62, and 63 samples of C1, C2, and C3, respectively. The nucleation rates were 98.6, 49.2, and 62.4 nuclei/L/min at C1, C2, and C3. A was determined as 1.0251, and B was calculated as −0.0675. The plot of nucleation rate J versus the supersaturation index (Figure 4E) was nonlinear, indicating deviation from classical nucleation theory. Nucleation rates decreased from C1 to C2 and increased from C2 to C3. Plot of ln J versus $\ln^{-2} S$ (Figure 4F) showed large deviations from linearity at the observed supersaturation levels. The deviation in linearity and hence from CNT depicts the deviation in precipitation behavior of CEL at higher supersaturation level. This relative stabilization of supersaturation at higher supersaturation levels may be attributed to the formation of molecular assemblies of CEL unbound by lattice energies in BNC milieu.[42,43]

In FeSSIF-v2, no precipitation was observed for C1, while C2 showed a subtle decrease in absorbance followed by an increase, indicating dissolution of CEL (Figure 5B). While C3 showed a steady decline in absorbance until the observed time. TPD plots could not be plotted for C1 and C2 due to the absence of precipitation. Prima facie, TPD of C3 in FeSSIF-v2 (Figure 5A), showed all colors, reflecting precipitation to some extent occurring in all time spans. The arrangement of precipitation distribution in increasing order of the first quarter precipitation showed an exponential pattern. Quantification of the nucleation rate for only C3 with 29 of the 88 samples shows precipitation of more than 90% in 70 min, thereby giving a value of 18.4 nuclei/L/min.

Metastable zone width (MSZW) for CEL was attempted through mean absorbance values of desupersaturation curves in different media to examine the impact of different media on MSZW of CEL. For reference, MSZW of CEL in water was

DOI: 10.1021/acs.molpharmaceut.8b00267
Mol. Pharmaceutics 2018, 15, 2423−2436

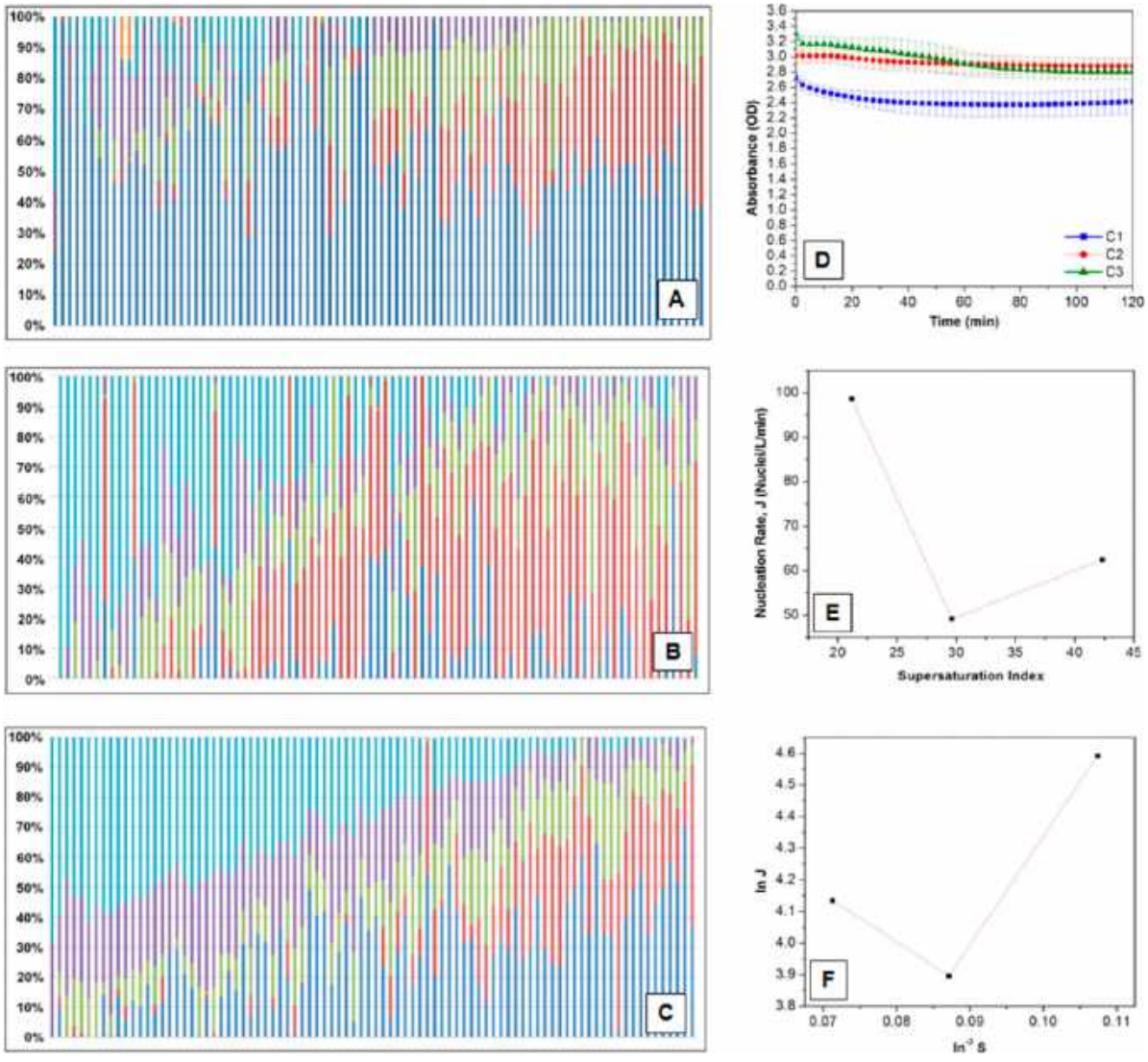

Figure 4. TPD diagrams in BNC of 88 samples each at three supersaturation indices (A) C1, (B) C2, and (C) C3 depicting the time-wise percentage of precipitation; dark blue for 0−15 min, red for 15−30 min, green for 30−45 min, purple for 45−60 min, cyan for 60−120 min, orange for 120−180 min, and light blue for 180−240 min. (D) Mean desupersaturation plots of C1, C2, and C3 in BNC. (E) Plot of nucleation rate J at different supersaturation indices. (F) Plot of ln J and $\ln^{-2} S$.

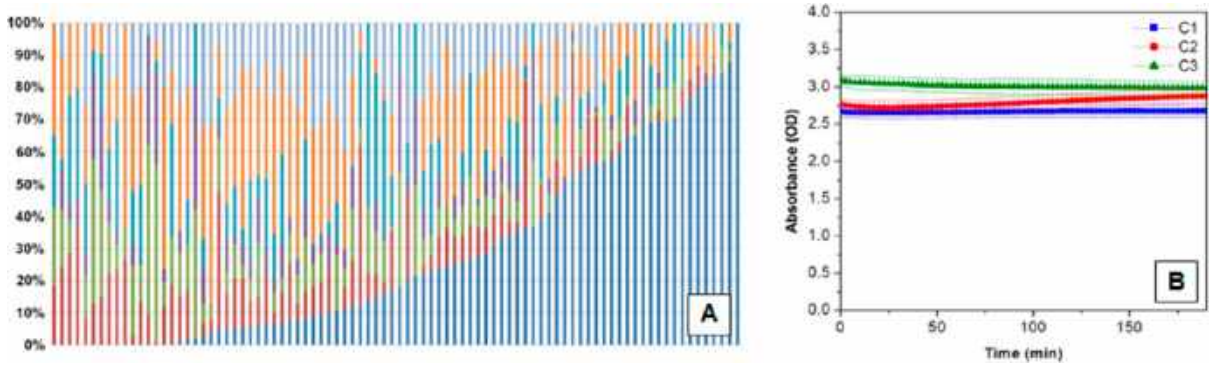

Figure 5. (A) TPD diagrams in FeSSIF-v2 of 88 samples at C3 depicting the time-wise percentage of precipitation; dark blue for 0−15 min, red for 15−30 min, green for 30−45 min, purple for 45−60 min, cyan for 60−120 min, orange for 120−180 min, and light blue for 180−240 min. (B) Mean desupersaturation plots of C1, C2, and C3 in FeSSIF-v2.

plotted and is represented as a pink shaded region in Figure 6. Broader MSZW signifies a greater degree of stabilization of solute in its supersaturated state. The MSZW decreased to a considerable extent in fasted state media of gastric and intestinal conditions as is indicated by the orange arrows. With the same amount of spiked drug, the peak level of

DOI: 10.1021/acs.molpharmaceut.8b00267
Mol. Pharmaceutics 2018, 15, 2423−2436

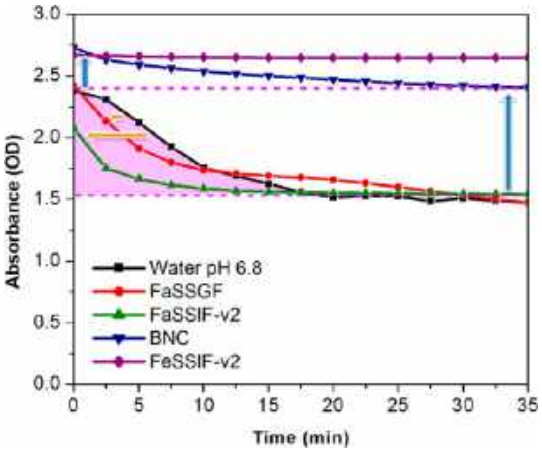

Figure 6. MSZW of CEL in different media.

supersaturation generated initially was less in FaSSIF-v2 than FaSSGF indicating the short-lived nature of CEL supersaturation in the intestinal environment. The fed state media increased the MSZW as indicated by blue lines. MSZW can be arranged in increasing order as FaSSIF-v2 < FaSSGF < water < BNC < FeSSIF-v2. This observation directs its implication in the drug delivery due to ensuing permeability enhancement of supersaturated drug. With fed state media showing stabilization of the supersaturated state of CEL for the period of observation, it thereby shows a positive interplay between food and supersaturation, which can explain the food effect observed with CEL. A directive obtained from this comparison would be to lookout for strategies that prevent precipitation of CEL in the fasted state media. An excipient capable of maintaining supersaturation in fasted media would lead to success of a delivery advantage from an SDDS of CEL.

Compositional Effect. The spiked drug seemed to have remained stable in its supersaturated state in water at pH 6.8 for nearly 5 min at the concentration of 129.0 μg/mL, then decreased at a linear rate. The nucleation rates calculated using the in-house criteria are enlisted in Table 3. At pH 1.6, the

Table 3. Nucleation Rates in Various Media Components

media component	$N(t)$	time (t) (min)	nucleation rate (J) (nuclei/L/min)
water	0.5455	17.5	145.3562
pH 1.6	0.4773	10	209.2734
sodium taurocholate 80 μM	0.7841	10	494.4968
sodium taurocholate 2 mM	0.5	30	74.53195
lecithin 20 μM	0.5795	5	558.9102
lecithin 0.2 mM	0.5568	20	131.2474
pepsin at pH 1.6	0.6136	5	613.4724

media does not have the capacity to retain CEL in a supersaturated state and led to a rapid fall in its levels (Figure 7A). Considering solubilization phenomenon, a result of formation of hydration shells of CEL, the presence of protons seems to affect the supersaturation holding capacity of the media by making water molecules less available for formation of hydration shells. Submicellar concentration of sodium taurocholate, seemed to have maintained the supersaturation levels of CEL for the same time as water, but the desupersaturation seemed faster as is reflected from the desupersaturation curve

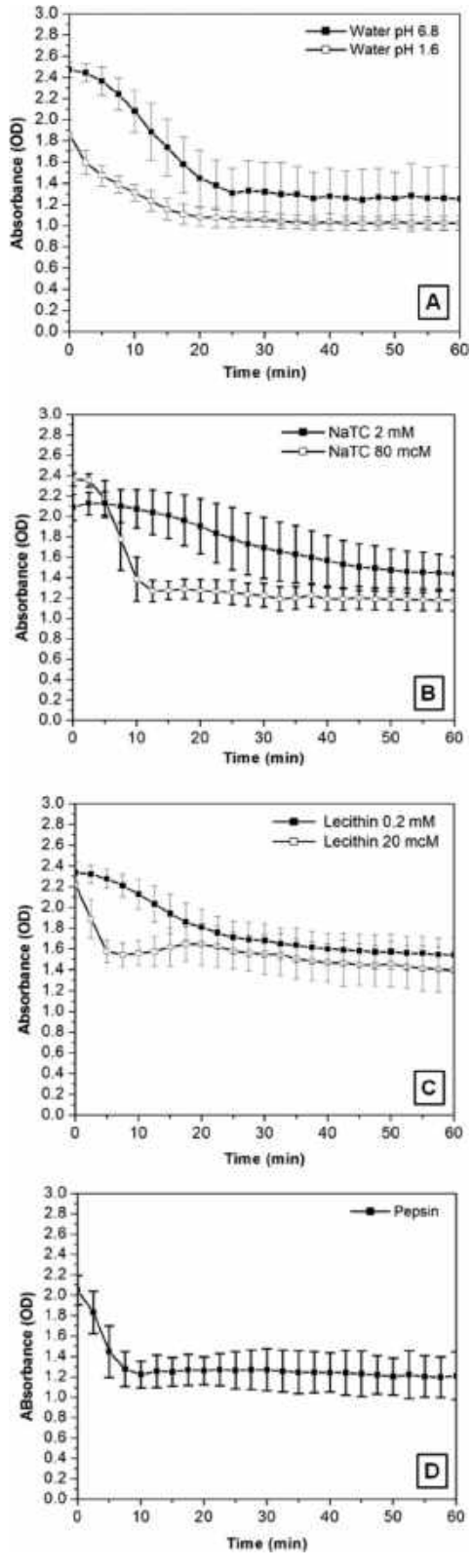

Figure 7. Desupersaturation profiles of CEL in various components of biorelevant media.

and nucleation rates. The micellar concentration of sodium taurocholate stabilized supersaturation. Further, a higher trough level of CEL could be observed at the end of the observation time, which can be attributed to micellar solubilization (Figure 7B). The gastric levels of lecithin destabilize supersaturation of

DOI: 10.1021/acs.molpharmaceut.8b00267
Mol. Pharmaceutics 2018, 15, 2423−2436

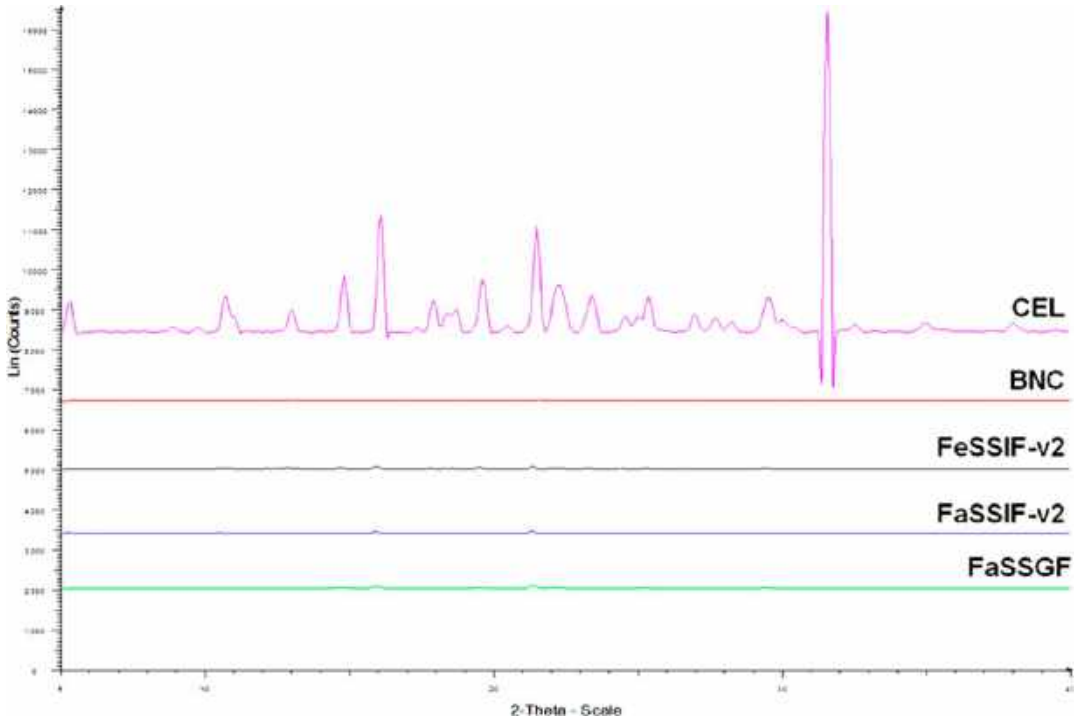

Figure 8. Overlay of PXRD patterns of precipitates with crystalline CEL as reference.

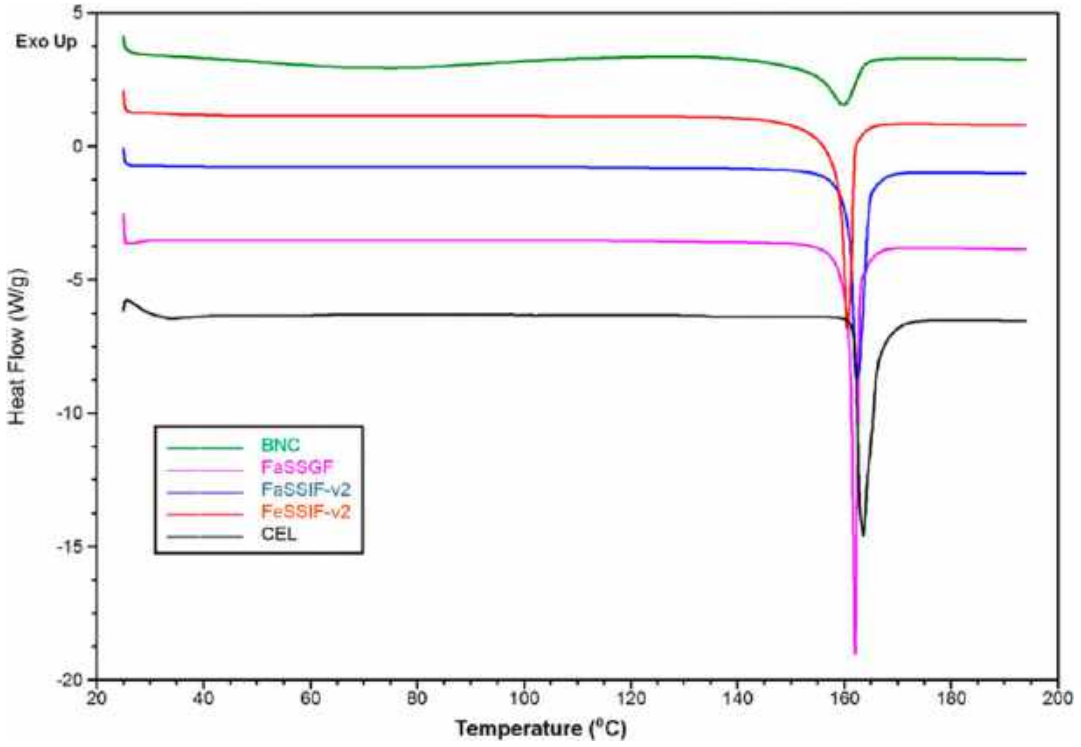

Figure 9. DSC endotherms of CEL and precipitates from different media.

CEL when compared to water also indicated by rapid precipitation and higher nucleation rate, while intestinal lecithin concentration (fasted level) seems to support supersaturation as well as solubilization (Figure 7C). Pepsin at pH 1.6 showed destabilization of the metastable supersaturated state (Figure 7D).

ADMET Predictor calculates a compound's supersaturation tendency on the basis of the ratio of its kinetic solubility over its intrinsic solubility with the threshold ratio being 1.3. ADMET Predictor showed CEL having a tendency to supersaturate in water, which complied with experimental observations.

Solid State Analysis. PXRD patterns of precipitates (Figure 8) reflected their crystalline nature. The characteristic peak of CEL at $2\theta = 5.5$ was remarkable in all precipitates. The other prominent peaks in the FaSSGF PXRD pattern were at 2θ values of 3.03570, 3.52028, 4.02648, 4.15885, 4.54340, and

DOI: 10.1021/acs.molpharmaceut.8b00267
Mol. Pharmaceutics 2018, 15, 2423−2436

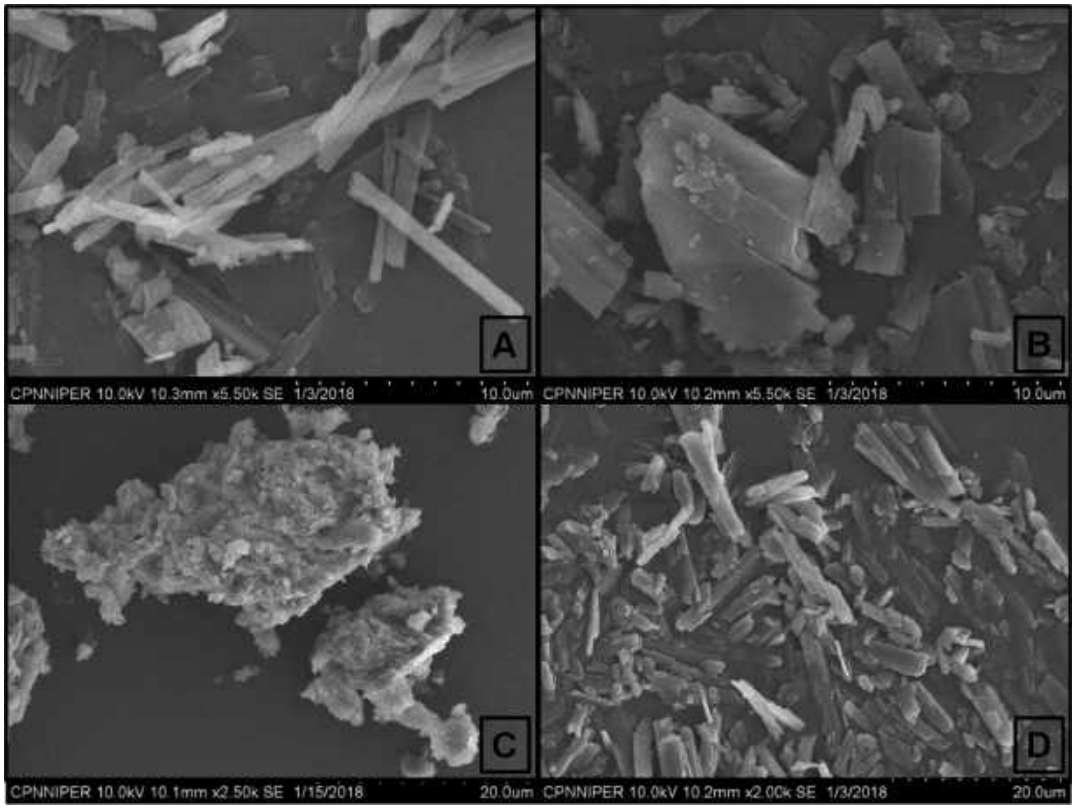

Figure 10. SEM images of CEL precipitates from (A) FaSSGF, (B) FaSSIF-v2, (C) BNC, and (D) FeSSIF-v2.

6.03245. FaSSIF-v2 precipitates showed peaks at 3.03858, 3.32694, 4.16711, 6.05111, and 8.44687. Prominent peaks in BNC precipitates can be demarcated at 2θ values of 3.45115, 4.12219, 4.28525, 4.96510, 5.98272, and 6.34213. In the PXRD pattern of FeSSIF-v2 precipitates, major peaks were present at 3.03487, 3.52509, 3.81059, 4.16418, 4.55255, 6.04168, and 6.89789. PXRD patterns confirmed the absence of any metastable or amorphous polymorph in the reprecipitated drug. The similarity of prominent peaks in the diffraction pattern of precipitates with pure CEL was directed toward the presence of the same polymorph in all samples.[44]

DSC (Figure 9) of precipitates from all media showed the presence of crystalline polymorph of CEL as all the precipitates showed a melting endotherm in the same range. However, shifts in onset of melting endotherm from pure CEL (onset at 162 °C) were observed for all precipitates with the maximum difference in BNC (onset: 153 °C) and minimum in FaSSIF-v2 precipitates (160 °C). The precipitates showed slight shift in endotherm as compared to pure CEL (form III). BNC precipitates showed suppression of the melting endotherm, while the same was enhanced for FaSSGF precipitates. These results indicate the influence of media components in the precipitation behavior of CEL, which can be observed through enthalpic behavior of melting of the precipitates. Enthalpic behavior of melting confirms the absence of any amorphous form being present in precipitates of CEL.

SEM images (Figure 10) showed morphological differences among precipitates of CEL from various biorelevant media. Precipitates from FaSSGF (Figure 10A) were long and needle-shaped indicating growth of crystals in only one direction. The surface of needles was mostly smooth. However, aggregation of needles was visible at some places. In FaSSIF-v2 (Figure 10B), broad flakes of crystals could be observed with fractures that might have developed during the drying stage. There were visible signs of secondary nucleation with the crystals formed during heterogeneous nucleation being quite smaller than the flakes. Precipitate from BNC (Figure 10C) was large and with irregular shape. Smaller but more numerous crystals observed in FeSSIF-v2 (Figure 10D) showed the availability of more sites where cluster formation took place during the nucleation stage. Particles were wider and uniform with visible aggregation.

Optical Microscopy. In FaSSGF, phase separation could be observed initially (Figure 11a) followed by the rapid growth of needle-like crystals aligning into a floral pattern (Figure 11b). There were dense clusters observable at places. Birefringence could be observed as tiny specks (Figure 11c). Following spiking of CEL in FaSSIF-v2, tiny needle-like scattered crystals could be observed initially (Figure 11d), which increased in number with time (Figure 11e). Floral clusters could be observed at some places. An increase in the applied drug concentration increased the number of scattered needles. Observation under polarized light showed birefringence in the form of needles (Figure 11f). Precipitation in BNC was observed as steady densification of zones (Figure 11g,h). Regular-shaped particles were not observed. Birefringence was observed mostly as tiny spots with elongated ones at places (Figure 11i). Introduction of CEL in FeSSIF-v2 led to the formation of a network of small globules (Figure 11j). Needles could be observed within the globular matrix after some time (Figure 11k), which showed birefringence (Figure 11l) when viewed under polarized light. These observations show that the precipitation of CEL under biorelevant conditions results in the direct generation of the crystalline CEL without any generation of amorphous CEL.

DOI: 10.1021/acs.molpharmaceut.8b00267
Mol. Pharmaceutics 2018, 15, 2423−2436

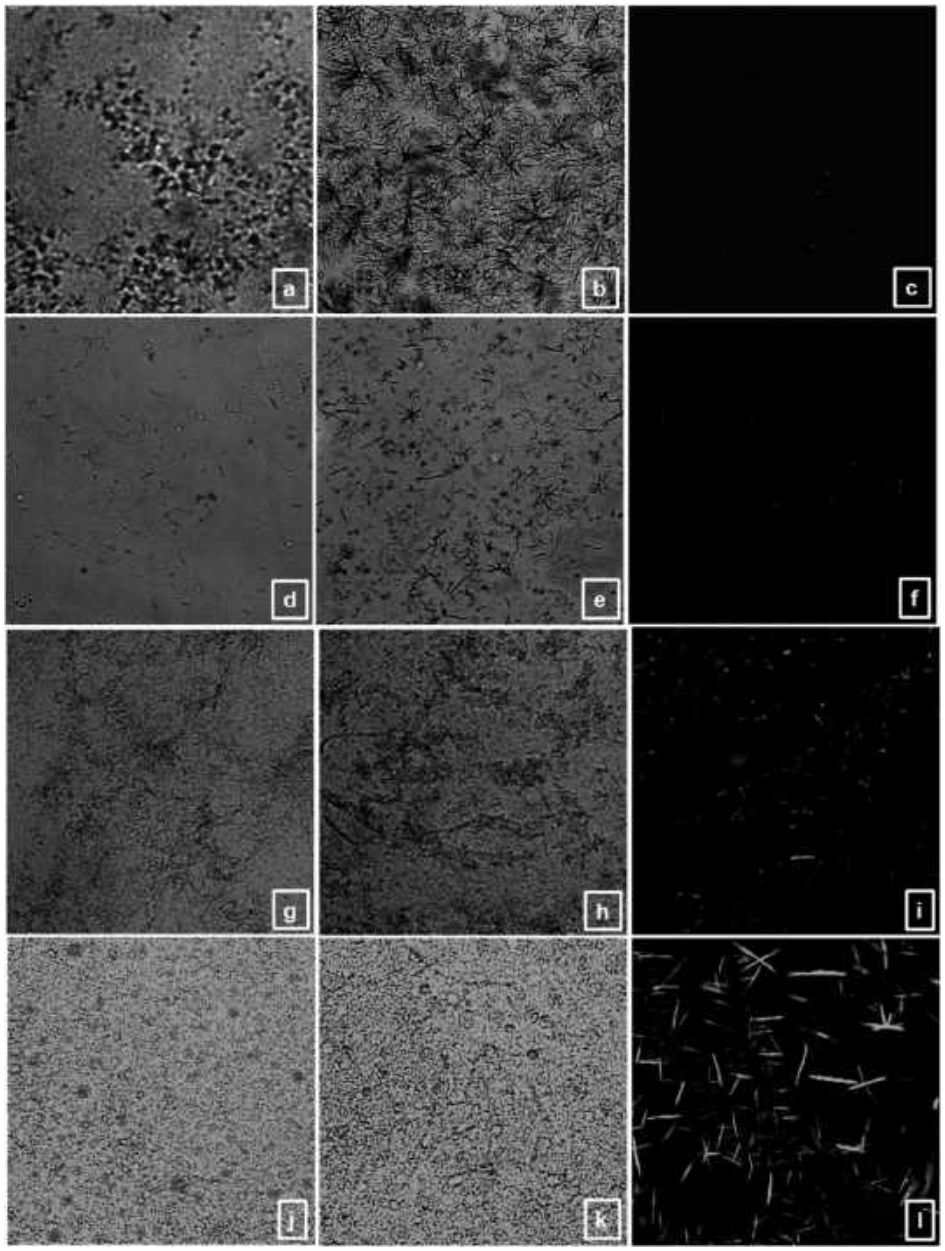

Figure 11. Photomicrography of precipitation (under 10× objective) in [a–c] FaSSGF; [d–f] FaSSIF-v2; [g–i] BNC, and [j–l] FeSSIF-v2 with [c], [f], [i], and [l] being birefringence of precipitates under polarized light.

CONCLUSION

Gastrointestinal precipitation of drugs can limit the supersaturation advantage of drugs with poor solubility. The process of precipitation is sensitive to composition and conditions of media, and in order to understand the *in situ* precipitation behavior of drugs, it is important to make the test media as biorelevant as possible. This study aimed to understand the precipitation profile of a BCS class II drug under biorelevant conditions in a comprehensive manner. Pursuing the principle of miniaturization for supersaturation assays while considering the stochastic nature of nucleation, the microarray plate method was developed and used the solvent shift methodology and spectrophotometric assay to study the precipitation kinetics. Assessments of precipitation profiles were made in biorelevant media representing fasted state and fed state conditions of the gastrointestinal tract. Application of CNT for quantification was done with the aim to understand the behavior of the precipitation of a model drug under different conditions with reference to a standard equation and demarcate deviations from it. Tailored criteria were employed due to nonapplicability of parameter "induction time" for cases of rapid precipitation and in cases where some degree of supersaturation stabilization occurs midway of desupersaturation profile. The criteria employed are not much different from induction time attributing to the fact that both encompass a fraction of crystal growth time. Precipitation followed a linear pattern for all concentrations in the case of FaSSGF and FaSSIF-v2, while a nonlinear pattern was observed for BNC. Quantification in the case of FeSSIF-v2 was done only for C3 as it could be discerned as the case of true supersaturation. An approach was made to visually represent the degree of precipitation in all samples of microarray plate through two-dimensional plots termed as "temporal precipitation distribu-

DOI: 10.1021/acs.molpharmaceut.8b00267
Mol. Pharmaceutics 2018, 15, 2423–2436

tion" plots. These plots help in quick recognition of the time interval of maximum precipitation and degree of supersaturation stabilization in all samples. Media representing fasted state gastric and intestinal conditions did not show stabilization of the supersaturated state of CEL and precipitated rapidly, while media representing fed state showed stabilization of a supersaturated state in terms of both nucleation rates and MSZW. Stabilization of a supersaturated state in BNC and FeSSIF-v2 with food-mediated solubilization can explain the food effect observed in the case of CEL. In order to understand the compositional effect of biorelevant media, supersaturation stability of CEL was assessed at gastric pH, in different concentrations of sodium taurocholate and lecithin and in pepsin individually. CEL, a drug with pH independent solubility, was documented to have pH-dependent supersaturation stability. Intestinal concentrations of sodium taurocholate and lecithin had a stabilizing impact on supersaturation of CEL, while notable destabilization was observed at their gastric concentrations. Pepsin, as an enzyme at pH 1.6, destabilized supersaturation. As reference, water showed supersaturation stabilization for CEL to a certain extent. A compositional effect study can help in identifying a biorelevant component that does not support supersaturation of a drug and can be used for designing media for supersaturation assay of drug for excipient screening. This methodology would eliminate the stabilization attributed by water while accentuating the unfavorable *in vivo* factor. Solid state characterization of precipitates was aimed to understand the nature of precipitates generated under biorelevant conditions. Though different media had some effect on the precipitation process as revealed by different morphologies and slight difference in onset of melting endotherms in DSC, the polymorphic form present in precipitates was crystalline of CEL. Optical microscopy of the precipitation process confirmed the direct generation of crystalline drug and ruled out formation of an amorphous form or polymorph transformation of CEL during precipitation. Development of supersaturation assay methodology for understanding precipitation under biorelevant conditions would require media that are suitable for spectrophotometric or visual supersaturation assays. BNC is a step in this direction, which was formulated from three basic components of food dissolved while having minimum optical absorbance. The media gives a good preliminary idea of interplay between food and supersaturated state of drug.

Absorption of BCS class II drugs is limited by their solubility. If supersaturating formulations deliver higher intraluminal drug concentration, then precipitation of the dissolved step becomes the limiting factor in absorption, thereby limiting their bioavailability. A comprehensive and systematic approach to understand the degree of precipitation and nature of precipitates would help in prospective identification of the site and extent where the drug delivery system would fail in delivering the supersaturated levels from an SDDS. Such a prospective analysis would help in designing formulations in an informed manner, which is highly required to be incorporated in the expensive process of drug development.

■ ASSOCIATED CONTENT

Supporting Information

The Supporting Information is available free of charge on the ACS Publications website at DOI: 10.1021/acs.molpharmaceut.8b00267.

Analytical method of CEL and its calibration curve developed using HPLC-PDA and individual PXRD patterns of precipitates of CEL from different media (PDF)

■ AUTHOR INFORMATION

Corresponding Author

*Tel: +91-0172 2214682. Fax: +91-0172 2214692. E-mail: abhays@niper.ac.in or abhaysangamwar@gmail.com.

ORCID

Abhay T. Sangamwar: 0000-0002-2331-1421

Notes

The authors declare no competing financial interest.

■ ACKNOWLEDGMENTS

We are thankful to NIPER, SAS Nagar for a fellowship and provision of infrastructural support for carrying out the study. We are grateful to Dr. Arvind Kumar Bansal and Dr. Sanyog Jain for extending support through DSC and SEM facilities, respectively. We also acknowledge Ms. Shamandeep Kaur and Mr. Sumit Mukesh for their valuable help.

■ REFERENCES

(1) Kalepu, S.; Nekkanti, V. Insoluble drug delivery strategies: review of recent advances and business prospects. *Acta Pharm. Sin. B* **2015**, *5* (5), 442−53.

(2) Parkash, V.; Maan, S.; Deepika; Yadav, S. K.; Hemlata; Jogpal, V. Fast disintegrating tablets: Opportunity in drug delivery system. *J. Adv. Pharm. Technol. Res.* **2011**, *2* (4), 223−235.

(3) Brouwers, J.; Brewster, M. E.; Augustijns, P. Supersaturating drug delivery systems: the answer to solubility-limited oral bioavailability? *J. Pharm. Sci.* **2009**, *98* (8), 2549−72.

(4) Guzmán, H.; Tawa, M.; Zhang, Z.; Ratanabanangkoon, P.; Shaw, P.; Mustonen, P.; Gardner, C.; Chen, H.; Moreau, J.-P.; Almarsson, O.; Remenar, J. Spring and parachute approach to designing solid celecoxib formulations having enhanced oral absorption. *AAPS J.* **2004**, T2189.

(5) Guzmán, H. R.; Tawa, M.; Zhang, Z.; Ratanabanangkoon, P.; Shaw, P.; Gardner, C. R.; Chen, H.; Moreau, J. P.; Almarsson, O.; Remenar, J. F. Combined Use of Crystalline Salt Forms and Precipitation Inhibitors to Improve Oral Absorption of Celecoxib from Solid Oral Formulations. *J. Pharm. Sci.* **2007**, *96* (10), 2686−2702.

(6) Taylor, L. S.; Zhang, G. G. Z. Physical chemistry of supersaturated solutions and implications for oral absorption. *Adv. Drug Delivery Rev.* **2016**, *101*, 122−142.

(7) Frank, K. J.; Rosenblatt, K. M.; Westedt, U.; Holig, P.; Rosenberg, J.; Magerlein, M.; Fricker, G.; Brandl, M. Amorphous solid dispersion enhances permeation of poorly soluble ABT-102: true supersaturation vs. apparent solubility enhancement. *Int. J. Pharm.* **2012**, *437* (1−2), 288−93.

(8) Raina, S. A.; Zhang, G. G. Z.; Alonzo, D. E.; Wu, J.; Zhu, D.; Catron, N. D.; Gao, Y.; Taylor, L. S. Enhancements and limits in drug membrane transport using supersaturated solutions of poorly water soluble drugs. *J. Pharm. Sci.* **2013**, *103* (9), 2736−2748.

(9) Beig, A.; Fine-Shamir, N.; Lindley, D.; Miller, J. M.; Dahan, A. Advantageous Solubility-Permeability Interplay When Using Amorphous Solid Dispersion (ASD) Formulation for the BCS Class IV P-gp Substrate Rifaximin: Simultaneous Increase of Both the Solubility and the Permeability. *AAPS J.* **2017**, *19* (3), 806−813.

(10) Dahan, A.; Beig, A.; Ioffe-Dahan, V.; Agbaria, R.; Miller, J. M. The twofold advantage of the amorphous form as an oral drug delivery practice for lipophilic compounds: increased apparent solubility and drug flux through the intestinal membrane. *AAPS J.* **2013**, *15* (2), 347−53.

(11) Gao, P.; Rush, B. D.; Pfund, W. P.; Huang, T.; Bauer, J. M.; Morozowich, W.; Kuo, M. S.; Hageman, M. J. Development of a supersaturable SEDDS (S-SEDDS) formulation of paclitaxel with improved oral bioavailability. *J. Pharm. Sci.* **2003**, *92* (12), 2386−98.
(12) Gupta, S.; Kesarla, R.; Omri, A. Formulation strategies to improve the bioavailability of poorly absorbed drugs with special emphasis on self-emulsifying systems. *ISRN Pharm.* **2013**, *2013*, 848043.
(13) Miller, J. M.; Beig, A.; Carr, R. A.; Spence, J. K.; Dahan, A. A win-win solution in oral delivery of lipophilic drugs: supersaturation via amorphous solid dispersions increases apparent solubility without sacrifice of intestinal membrane permeability. *Mol. Pharmaceutics* **2012**, *9* (7), 2009−16.
(14) Warren, D. B.; Benameur, H.; Porter, C. J. H.; Pouton, C. W. Using polymeric precipitation inhibitors to improve the absorption of poorly water-soluble drugs: A mechanistic basis for utility. *J. Drug Target.* **2010**, *18* (10), 704−731.
(15) Leyssens, T.; Baudry, C.; Escudero Hernandez, M. L. Optimization of a Crystallization by Online FBRM Analysis of Needle-Shaped Crystals. *Org. Process Res. Dev.* **2011**, *15* (2), 413−426.
(16) Pandalaneni, K.; Amamcharla, J. K. Focused beam reflectance measurement as a tool for in situ monitoring of the lactose crystallization process. *J. Dairy Sci.* **2016**, *99* (7), 5244−5253.
(17) Alonzo, D. E.; Gao, Y.; Zhou, D.; Mo, H.; Zhang, G. G. Z.; Taylor, L. S. Dissolution and Precipitation Behavior of Amorphous Solid Dispersions. *J. Pharm. Sci.* **2011**, *100* (8), 3316−3331.
(18) Wilson, W. W. Monitoring crystallization experiments using dynamic light scattering: Assaying and monitoring protein crystallization in solution. *Methods* **1990**, *1* (1), 110−117.
(19) Chavan, R. B.; Thipparaboina, R.; Kumar, D.; Shastri, N. R. Evaluation of the inhibitory potential of HPMC, PVP and HPC polymers on nucleation and crystal growth. *RSC Adv.* **2016**, *6* (81), 77569−77576.
(20) Prasad, D.; Chauhan, H.; Atef, E. Role of Molecular Interactions for Synergistic Precipitation Inhibition of Poorly Soluble Drug in Supersaturated Drug-Polymer-Polymer Ternary Solution. *Mol. Pharmaceutics* **2016**, *13* (3), 756−765.
(21) Bevernage, J.; Brouwers, J.; Clarysse, S.; Vertzoni, M.; Tack, J.; Annaert, P.; Augustijns, P. Drug supersaturation in simulated and human intestinal fluids representing different nutritional states. *J. Pharm. Sci.* **2010**, *99* (11), 4525−34.
(22) Almeida e Sousa, L.; Reutzel-Edens, S. M.; Stephenson, G. A.; Taylor, L. S. Supersaturation Potential of Salt, Co-Crystal, and Amorphous Forms of a Model Weak Base. *Cryst. Growth Des.* **2016**, *16* (2), 737−748.
(23) Chauhan, H.; Hui-Gu, C.; Atef, E. Correlating the Behavior of Polymers in Solution as Precipitation Inhibitor to its Amorphous Stabilization Ability in Solid Dispersions. *J. Pharm. Sci.* **2013**, *102* (6), 1924−1935.
(24) Ilevbare, G. A.; Liu, H.; Edgar, K. J.; Taylor, L. S. Maintaining Supersaturation in Aqueous Drug Solutions: Impact of Different Polymers on Induction Times. *Cryst. Growth Des.* **2013**, *13* (2), 740−751.
(25) Mellaerts, R.; Mols, R.; Kayaert, P.; Annaert, P.; Van Humbeeck, J.; Van den Mooter, G.; Martens, J. A.; Augustijns, P. Ordered mesoporous silica induces pH-independent supersaturation of the basic low solubility compound itraconazole resulting in enhanced transepithelial transport. *Int. J. Pharm.* **2008**, *357* (1−2), 169−79.
(26) Ozaki, S.; Minamisono, T.; Yamashita, T.; Kato, T.; Kushida, I. Supersaturation-nucleation behavior of poorly soluble drugs and its impact on the oral absorption of drugs in thermodynamically high-energy forms. *J. Pharm. Sci.* **2011**, *101* (1), 214−22.
(27) Yamashita, T.; Ozaki, S.; Kushida, I. Solvent shift method for anti-precipitant screening of poorly soluble drugs using biorelevant medium and dimethyl sulfoxide. *Int. J. Pharm.* **2011**, *419* (1), 170−174.
(28) Chait, A.; DeLucas, L.; Stoops, B.; Belgovskiy, A. Method for preparation of microarrays for screening of crystal growth conditions. U.S. Patent 7,244,396, July 17, 2007.
(29) Hu, Q.; Wyttenbach, N.; Shiraki, K.; Choi, D. S. Miniaturized Screening Tools for Polymer and Process Evaluation. In *Amorphous Solid Dispersions: Theory and Practice*; Shah, N., Sandhu, H., Choi, D. S., Chokshi, H., Malick, A. W., Eds.; Springer: New York, 2014; pp 165−195.
(30) Dai, W. G.; Dong, L. C.; Shi, X.; Nguyen, J.; Evans, J.; Xu, Y.; Creasey, A. A. Evaluation of drug precipitation of solubility enhancing liquid formulations using milligram quantities of a new molecular entity (NME). *J. Pharm. Sci.* **2007**, *96* (11), 2957−2969.
(31) Morrison, J. S.; Nophsker, M. J.; Haskell, R. J. A Combination Turbidity and Supernatant Microplate Assay to Rank Order the Supersaturation Limits of Early Drug Candidates. *J. Pharm. Sci.* **2014**, *103* (10), 3022−3032.
(32) Trifkovic, M.; Sheikhzadeh, M.; Rohani, S. Determination of metastable zone width for combined anti-solvent/cooling crystallization. *J. Cryst. Growth* **2009**, *311* (14), 3640−3650.
(33) Yu, J.; Li, A.; Chen, X.; Chen, Y.; Xie, J.; Wu, J.; Ying, H. Experimental Determination of Metastable Zone Width, Induction Period, and Primary Nucleation Kinetics of Cytidine 5-Monophosphate Disodium Salt in an Ethanol-Aqueous Mixture. *J. Chem. Eng. Data* **2013**, *58* (5), 1244−1248.
(34) Ulrich, J.; Strege, C. Some aspects of the importance of metastable zone width and nucleation in industrial crystallizers. *J. Cryst. Growth* **2002**, *237*−*239*, 2130−2135.
(35) Hens, B.; Pathak, S. M.; Mitra, A.; Patel, N.; Liu, B.; Patel, S.; Jamei, M.; Brouwers, J.; Augustijns, P.; Turner, D. B. In Silico Modeling Approach for the Evaluation of Gastrointestinal Dissolution, Supersaturation, and Precipitation of Posaconazole. *Mol. Pharmaceutics* **2017**, *14* (12), 4321−4333.
(36) Jiang, S.; ter Horst, J. H. Crystal Nucleation Rates from Probability Distributions of Induction Times. *Cryst. Growth Des.* **2010**, *11* (1), 256−261.
(37) Krishnan, V.; Random Processes. In *Probability and Random Processes*; John Wiley & Sons, Inc., 2005; pp 406−489.
(38) Karthika, S.; Radhakrishnan, T. K.; Kalaichelvi, P. A Review of Classical and Nonclassical Nucleation Theories. *Cryst. Growth Des.* **2016**, *16* (11), 6663−6681.
(39) Paulson, S. K.; Vaughn, M. B.; Jessen, S. M.; Lawal, Y.; Gresk, C. J.; Yan, B.; Maziasz, T. J.; Cook, C. S.; Karim, A. Pharmacokinetics of celecoxib after oral administration in dogs and humans: effect of food and site of absorption. *J. Pharmacol. Exp. Ther.* **2001**, *297* (2), 638−45.
(40) Jantratid, E.; Dressman, J. Biorelevant Dissolution Media Simulating the Proximal Human Gastrointestinal Tract: An Update. *Dissolution Technol.* **2009**, *16* (3), 21−25.
(41) Dahan, A. S.; Amidon, G. L. Gastrointestinal Dissolution and Absorption of Class II Drugs. In *Drug Bioavailability*, 2nd ed.; Mannhold, R., Kubinyi, H., Folkers, G., van de Waterbeemd, H., Testa, B., Eds.; Wiley-VCH Verlag GmbH & Co. KGaA, 2009; pp 33−51.
(42) Li, Z.; Lenk, T. I.; Yao, L. J.; Bates, F. S.; Lodge, T. P. Maintaining Hydrophobic Drug Supersaturation in a Micelle Corona Reservoir. *Macromolecules* **2018**, *51* (2), 540−551.
(43) Mistry, P.; Mohapatra, S.; Gopinath, T.; Vogt, F. G.; Suryanarayanan, R. Role of the Strength of Drug-Polymer Interactions on the Molecular Mobility and Crystallization Inhibition in Ketoconazole Solid Dispersions. *Mol. Pharmaceutics* **2015**, *12* (9), 3339−3350.
(44) Lu, G. W.; Hawley, M.; Smith, M.; Geiger, B. M.; Pfund, W. Characterization of a novel polymorphic form of celecoxib. *J. Pharm. Sci.* **2006**, *95* (2), 305−317.

DOI: 10.1021/acs.molpharmaceut.8b00267
Mol. Pharmaceutics 2018, 15, 2423−2436